Global and Regional Aspects of Tropical Cyclone Activity in the CMIP5 Models

SUZANA J. CAMARGO

Lamont-Doherty Earth Observatory, Columbia University, Palisades, New York

(Manuscript received 31 July 2012, in final form 27 July 2013)

ABSTRACT

Tropical cyclone (TC) activity is analyzed in 14 models from phase 5 of the Coupled Model Intercomparison Project (CMIP5). The global TC activity in the historical runs is compared with observations. The simulation of TC activity in the CMIP5 models is not as good as in higher-resolution simulations. The CMIP5 global TC frequency is much lower than observed, and there is significant deficiency in the geographical patterns of TC tracks and formation. Although all of the models underestimate the global frequency of TCs, the models present a wide range of global TC frequency. The models with the highest horizontal resolution have the highest level of global TC activity, though resolution is not the only factor that determines model TC activity. A cold SST bias could potentially contribute to the low number of TCs in the models. The models show no consensus regarding the difference of TC activity in two warming scenarios [representative concentration pathway 4.5 (RCP4.5) and RCP8.5] and the historical simulation. The author examined in more detail North Atlantic and eastern North Pacific TC activity in a subset of models and found no robust changes across models in TC frequency. Therefore, there is no robust signal across the CMIP5 models in global and regional TC changes in activity for future scenarios. The future changes in various large-scale environmental fields associated with TC activity were also examined globally: genesis potential index, potential intensity, vertical wind shear, and sea level pressure. The multimodel mean changes of these variables in the CMIP5 models are consistent with the changes obtained in the CMIP3 models.

1. Introduction

There is a huge interest in the potential change of tropical cyclone behavior with global warming due to the large impacts of tropical cyclones on coastal communities around the world. Three approaches to inferring tropical cyclone (TC) activity from climate models are (i) to examine the statistics of TC-like storms generated by models, (ii) to analyze the large-scale variables associated with TC activity, or (iii) to perform statistical or dynamical downscaling, and each of these approaches has positive and negative aspects. In this paper, we will apply the first two approaches to data from the phase 5 of the Coupled Model Intercomparison Project (CMIP5) dataset (Taylor et al. 2012). First, we will examine the ability of the models to simulate TC-like storms and determine whether the models show robust global and regional responses to warming. Second, we analyze the changes in large-scale environmental variables associated with TCs.

Low-resolution climate models can generate TC-like structures (e.g., Manabe et al. 1970; Bengtsson et al. 1982; Vitart et al. 1997; Camargo et al. 2005). These model TCs have some characteristics similar to observed TCs, including temporal and spatial climatological distributions, but are much weaker and larger than observed storms owing to the low resolution; other issues in simulating TC-like storms in low-resolution models are discussed in McBride (1984). Even when the TC model mean frequency is not correctly simulated, these models are able to capture interannual variability associated with El Niño–Southern Oscillation (ENSO) and have been used successfully to develop dynamical (Vitart and Stockdale 2001; Camargo and Barnston 2009) and statistical–dynamical (Wang et al. 2009) seasonal forecasts of TC activity. More recently, multiyear hurricane forecasts have been developed using these models (Smith et al. 2010; Vecchi et al. 2013).

In the last few years, many centers have started to use high-resolution global climate models having more realistic TC characteristics (e.g., Bengtsson et al. 2007a,b;

Corresponding author address: Suzana J. Camargo, Lamont-Doherty Earth Observatory, Columbia University, P.O. Box 1000, Palisades, NY 10964-800.
E-mail: suzana@ldeo.columbia.edu

DOI: 10.1175/JCLI-D-12-00549.1

Gualdi et al. 2008; Zhao et al. 2009) across a range of time scales—including intraseasonal (Vitart 2009; Vitart et al. 2010; Jiang et al. 2012), seasonal (LaRow et al. 2008; Zhao et al. 2009; Chen and Lin 2011), and longer time scales—with considerable success (e.g., Oouchi et al. 2006; Chauvin et al. 2006; Sugi et al. 2009). In most cases, these simulations are forced with prescribed sea surface temperature (SST); only in a few cases are fully coupled models used (e.g., Gualdi et al. 2008). Not all of these high-resolution global models are able to simulate the most intense storms, and downscaling methods (statistical, dynamical, and statistical–dynamical) have been employed to obtain more detailed information about projected TC characteristics, especially intensity (Knutson et al. 2008; Bender et al. 2010; Lavender and Walsh 2011; Zhao and Held 2010; Villarini and Vecchi 2012, 2013). The most recent version of a Japanese model [Meteorological Research Institute atmospheric general circulation model (MRI-AGCM)] with 20-km resolution is able to simulate intense Category 4 and 5 TCs (Murakami et al. 2012b).

As low-resolution climate models are better able to simulate the large-scale environmental, rather than individual, storms, one attractive approach is to analyze large-scale variables known to be associated with TC activity, instead of model TCs directly. Gray (1979) first developed a genesis index based on four parameters associated with TC occurrence. Emanuel and Nolan (2004) improved the Gray index, and further refinements have been suggested by various authors (e.g., Emanuel 2010; Tippett et al. 2011; Bruyère et al. 2012). Although these indices have some issues (see, e.g., Menkes et al. 2012), the simplicity of these indices is their main attraction, and they have been applied to infer TC activity on various time scales, including intraseasonal (Camargo et al. 2009), seasonal (Camargo et al. 2007a; Yokoi et al. 2009), future climate change (Vecchi and Soden 2007b, hereafter VS07b; Yokoi and Takayabu 2009), and past climates (Korty et al. 2012a,b). Following the same principle used in the CMIP3 models (Vecchi and Soden 2007a, hereafter VS07a; VS07b), analysis of projected changes of TC activity were performed using large-scale environmental variables known to be associated with TC activity such as potential intensity, vertical wind shear, and humidity.

Given the scope of the CMIP5 experiment design, most modeling centers contributed output from fairly low-resolution models. Therefore, it is useful to consider the large-scale environmental changes in addition to model storms. We expect that the CMIP5 simulation of TC activity will not be as good as in high-resolution simulations, but want to know how close the CMIP5-class models are. We are particularly interested in whether the CMIP5 models project robust changes in the global TC activity similar to those seen in the high-resolution projections.

Until now, projected changes in TC activity are robust only on a global scale, with an expected small reduction in global TC frequency and a small increase in TC intensity by the end of the twenty-first century (Knutson et al. 2010). We want to know if the CMIP5 models reproduce these projected changes. We will also explore the robustness of regional changes in TC activity across CMIP5 models focusing on the North Atlantic and eastern North Pacific.

In section 2, we describe the models, data, and methods used in this paper. Section 3 discusses the global TC activity in the CMIP5 models, with a detailed analysis of TCs in the eastern North Pacific and North Atlantic region presented in section 4. The changes in large-scale environment from the end of the twentieth century to the end of the twenty-first century are presented in section 5. A discussion of the results of our analysis is given in section 6. A few of the results presented here also appear in the U.S. National Oceanic and Atmospheric Administration/Modeling Analysis and Prediction Program (MAPP) synthesis papers on North American climate in the CMIP5 models (Sheffield et al. 2013; Maloney et al. 2013, manuscript submitted to *J. Climate*).

2. Models, data, and methods

a. CMIP5 models

The choice of models used in this analysis was based on their data availability in the CMIP5 data portals (Taylor et al. 2012). Tracking TC-like storms in the models using the Camargo and Zebiak (2002) algorithm requires 6-hourly environmental variables (viz., vorticity at 850 hPa, temperature and winds on various pressure levels, and surface pressure), and this requirement was the main restriction in our model choices since not all models provided the necessary variables at this output frequency at the time of our analysis.

Furthermore, the data had to be accessible for specific scenarios [more details in Taylor et al. (2012)]. Our analysis includes a historical simulation and two future warming scenarios. The historical simulation is forced with observed atmospheric composition changes (natural and anthropogenic), as well as time-evolving land cover. The historical simulations are available from the mid-nineteenth century to the near present, but we restricted our analysis to the period 1950–2005. For the future scenarios, we chose two projection simulations forced with specified atmospheric concentrations, also called representative concentration pathways (RCPs). The first one is a midrange mitigation emissions scenario

TABLE 1. CMIP5 models used to track TC-like structures using 6-hourly data: model acronym, name, modeling center, and approximate horizontal resolution (Taylor et al. 2012).

Acronym	Model name	Number	Modeling center	Resolution	Reference or link
CanESM2	Second Generation Canadian Earth System Model	M1	Canadian Centre for Climate Modeling and Analysis	2.8° × 2.9°	http://www.ec.gc.ca
CCSM4	Community Climate System Model, version 4	M2	National Center for Atmospheric Research	1.2° × 0.9°	Gent et al. 2011
CSIRO Mk3.6.0	Commonwealth Scientific and Industrial Research OrganizationMark, version 3.6.0	M3	Commonwealth Scientific and Industrial Research Organization and Queensland Climate Change Centre of Excellence	1.9° × 1.9°	Rotstayn et al. 2012
FGOALS-g2	Flexible Global Ocean–Atmosphere–Land System Model gridpoint, version 2	M4	LASG, Institute of Atmospheric Physics, Chinese Academy of Sciences and CESS, Tsinghua University	2.8° × 3.0°	Bao et al. 2013
GFDL CM3	Geophysical Fluid Dynamics Laboratory Climate Model, version 3	M5	NOAA/Geophysical Fluid Dynamics Laboratory	2.5° × 2.0°	Donner et al. 2011
GFDL-ESM2M	Geophysical Fluid Dynamics Laboratory Earth System Model with Modular Ocean Model 4 (MOM4) component	M6	NOAA/Geophysical Fluid Dynamics Laboratory	2.5° × 2.0°	Donner et al. 2011
HadGEM2-ES	Hadley Centre Global Environment Model, version 2–Earth System	M7	Met Office Hadley Center	1.9° × 1.2°	Jones et al. 2011
INM-CM4.0	Institute of Numerical Mathematics Coupled Model, version 4.0	M8	Institute of Numerical Mathematics	2.0° × 1.5°	Volodin et al. 2010
IPSL-CM5A-LR	L'Institut Pierre-Simon Laplace Coupled Model, version 5, coupled with NEMO, low resolution	M9	L'Institut Pierre Simon Laplace	3.7° × 1.9°	Voldoire et al. 2013
MIROC-ESM	Model for Interdisciplinary Research on Climate, Earth System Model	M10	Japan Agency for Marine-Earth Science and Technology, Atmosphere and Ocean Research Institute (University of Tokyo), and National Institute for Environmental Studies	2.8° × 2.8°	Watanabe et al. 2011
MIROC5	Model for Interdisciplinary Research on Climate, version 5	M11	Japan Agency for Marine-Earth Science and Technology, Atmosphere and Ocean Research Institute (University of Tokyo), and National Institute for Environmental Studies	1.4° × 1.4°	Watanabe et al. 2010
MPI-ESM-LR	Max Planck Institute Earth System Model, low resolution	M12	Max Planck Institute for Meteorology	1.9° × 1.9°	Zanchettin et al. 2012
MRI-CGCM3	Meteorological Research Institute Coupled Atmosphere–Ocean General Circulation Model, version 3	M13	Meteorological Research Institute	1.1° × 1.2°	Yukimoto et al. 2012
NorESM1-M	Norwegian Earth System Model, version 1 (intermediate resolution)	M14	Norwegian Climate Centre	2.5° × 1.9°	Zhang et al. 2012

(RCP4.5), and the second a high emissions scenario (RCP8.5). To include a model in our analysis, we required 6-hourly data for the historical run as well as the RCP4.5 and/or RCP8.5 future scenarios. In Table 1 we list the models used in this study.

For the calculations based on monthly data (e.g., potential intensity, genesis potential index), we used all available ensemble members available, even if they were different than that used in tracking the cyclones. A list of the 14 models analyzed and number of ensemble

TABLE 2. CMIP5 models and number of ensemble members used to calculate 6-hourly and monthly mean environmental variables.

Model	Number	Storms tracking: 6-hourly data			Environmental fields: monthly data	
		Historical	RCP4.5	RCP8.5	Historical	RCP8.5
CanESM2	M1	1	1	1	5	5
CCSM4	M2	1	1	1	6	3
CSIRO Mk3.6.0	M3	1	1	1	10	5
FGOALS-g2	M4	2	0	1	5	1
GFDL CM3	M5	1	1	1	1	1
GFDL-ESM2M	M6	1	1	1	1	1
HadGEM2-ES	M7	1	1	1	4	4
INM-CM4.0	M8	1	1	1	1	1
IPSL-CM5A-LR	M9	1	1	1	5	4
MIROC-ESM	M10	1	1	1	3	1
MIROC5	M11	2	3	2	4	3
MPI-ESM-LR	M12	3	3	3	3	3
MRI-CGCM3	M13	5	1	1	4	1
NorESM1-M	M14	1	1	1	3	1

members used for 6-hourly and monthly data calculations is given in Table 2.

b. Data

The observed TCs data used in this paper are based on best-track datasets from the National Hurricane Center (North Atlantic and eastern North Pacific) and the Joint Typhoon Warning Center (western North Pacific, north Indian Ocean, and Southern Hemisphere) and are available online (Jarvinen et al. 1984; Neumann et al. 1999; Chu et al. 2002). The National Centers for Environmental Prediction–National Center for Atmospheric Research (NCEP–NCAR) reanalysis dataset was used in the calculation of the present climate genesis potential index (Kalnay et al. 1996; Kistler et al. 2001). The sea surface temperature from NOAA was also used in our analysis (Smith et al. 2008).

c. Methods

The Camargo–Zebiak detection and tracking algorithm was used to identify and track TC-like storms in the CMIP5 model 6-hourly output (Camargo and Zebiak 2002). This algorithm has been used extensively in global (e.g., Camargo et al. 2005; Walsh et al. 2010; Kim et al. 2012) and regional climate models (Landman et al. 2005; Camargo et al. 2007b) and operationally in the International Research Institute for Climate and Society (IRI) TC seasonal dynamical forecast (Camargo and Barnston 2009). Here the algorithm was slightly modified to use 850-hPa wind speed instead of surface wind speed and three instead of four temperature levels (850, 500, and 300 hPa) due to their unavailability in the CMIP5 6-hourly data.

The Camargo–Zebiak algorithm is an objective algorithm for detection and tracking of individual storms and

TABLE 3. Thresholds used for vorticity ($10^{-5}\,s^{-1}$), 850-hPa wind speed ($m\,s^{-1}$), and vertical integrated temperature anomaly (°C) for defining TC-like storms for all models in the western North Pacific. Also shown are global thresholds for the relaxed vorticity ($10^{-5}\,s^{-1}$) used to track the storms in the models, which are defined by the model resolution.

Model	Number	Thresholds			
		Vorticity	Wind speed	Temperature	Relaxed vorticity
CanESM2	M1	3.1	13.0	1.7	1.5
CCSM4	M2	3.8	12.9	1.2	3.5
CSIRO Mk3.6.0	M3	3.9	13.3	2.1	2.7
FGOALS-g2	M4	3.1	12.8	1.1	1.4
GFDL CM3	M5	3.4	13.4	2.0	2.0
GFDL-ESM2M	M6	3.1	11.3	3.0	2.7
HadGEM2-ES	M7	4.1	13.9	2.0	2.6
INM-CM4.0	M8	3.2	11.9	1.4	0.6
IPSL-CM5A-LR	M9	2.9	13.0	3.0	1.6
MIROC-ESM	M10	3.4	14.8	3.4	3.3
MIROC5	M11	3.9	11.7	1.4	2.7
MPI-ESM-LR	M12	3.6	12.8	1.9	3.5
MRI-CGCM3	M13	4.7	13.9	2.0	3.5
NorESM1-M	M14	3.1	12.8	1.1	2.0

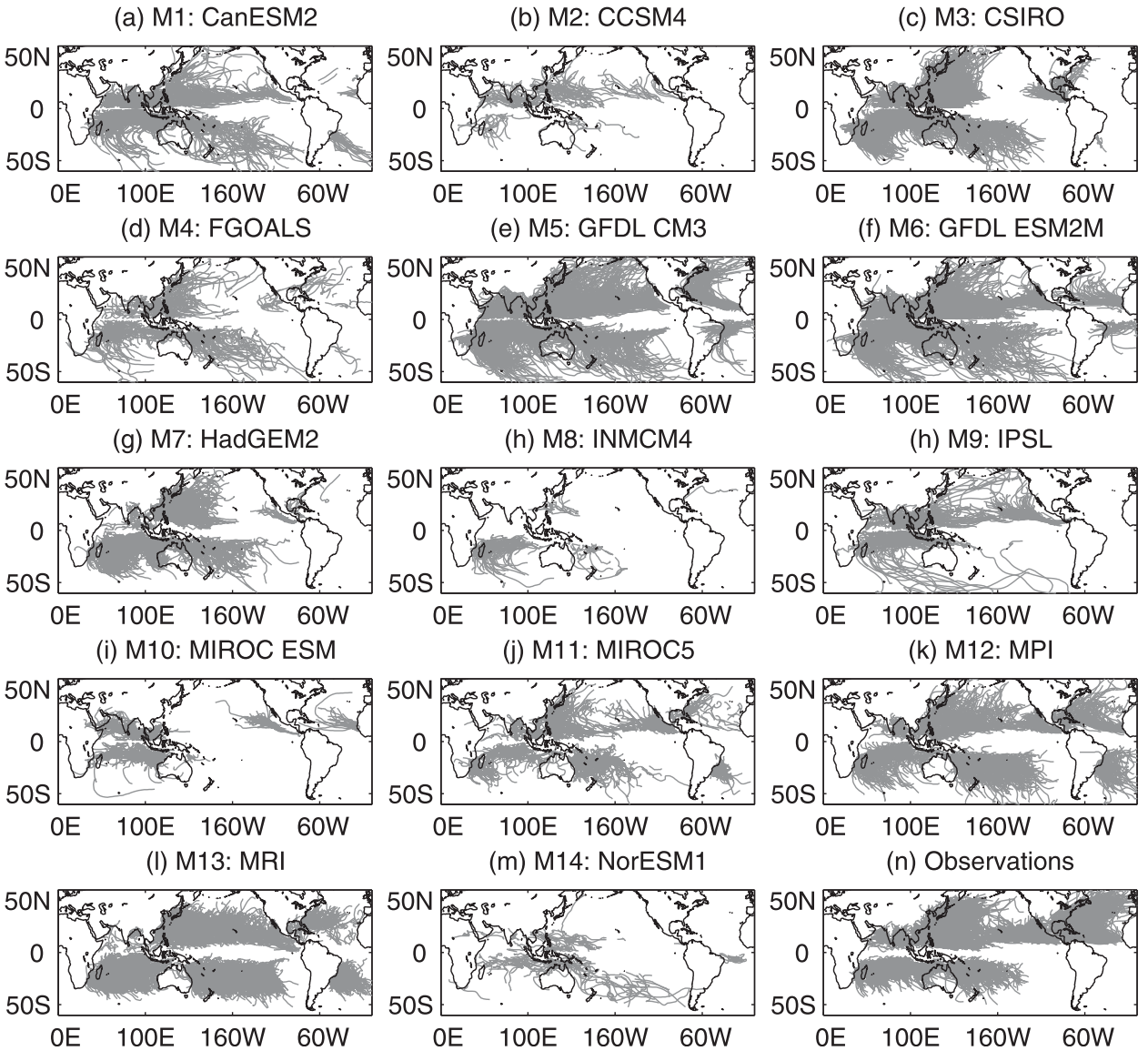

FIG. 1. TC tracks in 14 CMIP5 models (historical runs) and in observations for the period 1980–2005. Only one ensemble member is shown for each model.

was developed based, substantially, on prior studies (Bengtsson et al. 1995; Vitart et al. 1997). The algorithm detects and tracks structures with local maximum vorticity (850 hPa) and wind speed, minimum surface pressure, and a warm core (based on temperature and wind fields). To be defined as a model storm, the 6-hourly values of the vorticity, wind speed, and local temperature anomaly have to be above model and basin-dependent thresholds and last at least two days. The algorithm has two parts. In the detection part, vortices that meet environmental and duration criteria are identified. First, we identify grid points in the model 6-hourly output that are above specific dynamical and thermodynamical thresholds based on model climatology at each ocean basin in the present climate. Then potential storm locations that belong to the same storm are connected in time and space and only storms that last at least two days are considered. In the tracking part, the storm centers are first obtained from the vorticity centroid, which defines the center of the TC-like storm; the location magnitude of the vorticity centroid in the next (and previous) time steps in nearby grid points are found; and the process is repeated until the vorticity value is below a relaxed value for the vorticity threshold (lower than the vorticity threshold used in the detection part). The procedure is performed for all storms obtained using the

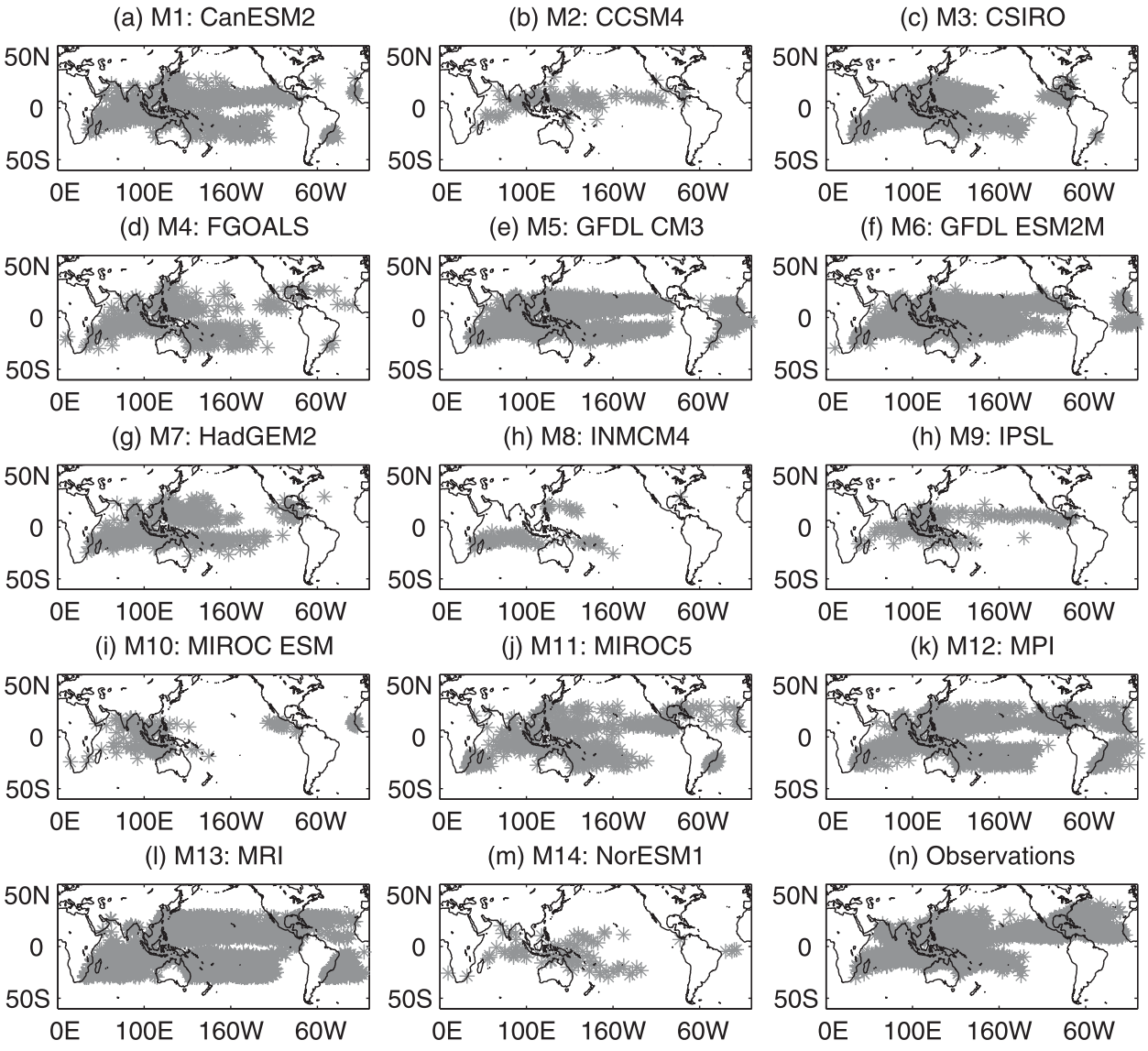

FIG. 2. TC first position in the tracks of 14 CMIP5 models (historical runs) and observations for the period 1980–2005 (shown in Fig. 1). Only one ensemble member is shown for each model.

detection algorithm. Then, the tracks obtained are compared to be sure that there are no repeated tracks.

These thresholds are based on statistics of the 6-hourly output of the historical runs. The definition of the thresholds was based on a study of the joint probability distribution of these environmental variables in a climate model (Camargo and Zebiak 2002). The vorticity threshold is defined as twice the vorticity standard deviation in each basin. The wind speed (for the CMIP5 models 850 hPa, usually 10 m or 1000 hPa) threshold is calculated as the sum of the oceanic global wind speed plus the wind speed standard deviation in each basin. The last threshold is for the vertically integrated local anomalous temperature T_v and is defined as the standard deviation of T_v in each basin. Although there is some spread of these thresholds in different basins, there are much larger differences among different models. The same thresholds are used for the future climate projection simulations. Once the vortex passes these criteria, the 6-hourly positions that belong to the same storm are identified and finally the track is extended in time backward and forward using a relaxed vorticity threshold.

These thresholds are defined objectively and quantitatively, so there is no ''tuning.'' There is a resolution dependence embedded in this algorithm as well, as the values of maximum vorticity, minimum sea level pressure,

and temperature anomaly are defined in a 5×5 gridpoint box, which is increased to 7×7 or 9×9 as the horizontal resolution increases. Values of the three thresholds for the 14 models analyzed in the western North Pacific in the present climate are given in Table 3 for comparison. The second relaxed threshold for the vorticity is global (i.e., the same for all basins) and is defined based on model resolution only (see Table 3), similar to the definition of the wind speed threshold given in Walsh et al. (2007). One advantage of this methodology is that there are no subjective definitions of the thresholds and all models are examined using exactly the same criteria for all. When comparing TC activity in models that are defined using different tracking routines, an objective comparison of the TC activity in these models would be dependent on the differences between these tracking routines.

Even imposing a warm core requirement on the storms, extratropical storms are not completely eliminated by our algorithm—a common problem in tracking algorithms (Horn et al. 2013). Therefore we impose an additional constraint here that we only consider storms forming in the tropics (30°S–30°N) over the ocean. It should be noted that, in contrast to the results showed here, in Sheffield et al. (2013) and Maloney et al. (2013, manuscript submitted to *J. Climate*) this additional tropical formation constraint was not imposed and a uniform (for all models) relaxed vorticity criteria with a value of $3.5 \times 10^{-5}\,\mathrm{s}^{-1}$ was used.

The genesis potential index (GPI) used here was developed in Emanuel and Nolan (2004) and discussed in detail in Camargo et al. (2007a). The GPI has been extensively applied and analyzed (e.g., Camargo et al. 2007e; Nolan et al. 2007; VS07a; Camargo et al. 2009; Tippett et al. 2011; Menkes et al. 2012). The GPI is a measure of potential formation of TCs based on four environmental variables: namely, low-level vorticity, vertical wind shear, midlevel relative humidity, and potential intensity. To facilitate comparison among the models, the GPI was calculated on a 2° latitude $\times$ 2° longitude grid for all models with all model fields being first interpolated to this grid before the GPI was calculated.

There are many possible genesis indices to choose from in the literature (e.g., Emanuel 2010; Tippett et al. 2011; Bruyère et al. 2012): a recent comparison of a few genesis indices is given in Menkes et al. (2012). There are indeed significant differences among them: in the case of Bruyère et al. (2012), for instance, with an index developed for the North Atlantic region, the moisture and vorticity are not considered to contribute to the capacity of the index in reproducing the number of storms in the region. In Tippett et al. (2011), however, with an index developed globally using different methodology, the analysis showed that there is a minimum amount of climatological vorticity necessary for the formation of storms but, once that amount is reached, increasing climatological vorticity does not lead to the formation of more storms. The reason why we chose the Emanuel and Nolan GPI, instead of any of the other indices, is for a more direct comparison with the results of CMIP3, as VS07a used this index in their analysis.

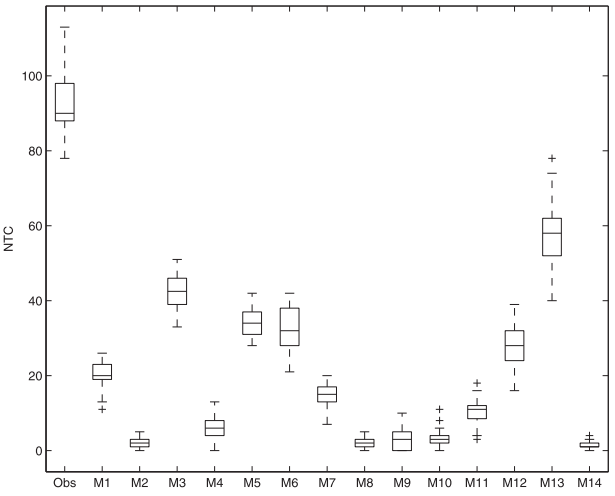

FIG. 3. Distribution of the global number of TCs per year in each of the models for the historical runs and in observations in the period 1980–2005. When more than one ensemble member is available, all ensemble members are used in the model distribution. The box denotes the range from the 25th to 75th percentile of the distributions, with the median marked by the line inside the box and the values outside of the middle quartile being marked by dashes and crosses.

Potential intensity (PI) is a theoretical limit for TC intensity (Emanuel 1988). The procedure for calculating the PI was first developed in Emanuel (1995) and later modified to take into account dissipative heating (Bister and Emanuel 1998, 2002a,b). The PI depends on sea surface temperature, sea level pressure, and profiles of temperature and humidity. PI has been extensively used as a proxy of TC intensity in analysis of low-resolution climate models (e.g., VS07b; Camargo et al. 2013), as local PI has a high correlation with actual TC intensities at various time scales (Emanuel 2000; Wing et al. 2007). Similarly to the case of the GPI, the PI was calculated on a $2° \times 2°$ uniform grid for all models.

The cluster analysis was developed in Gaffney (2004) and is described in detail in Gaffney et al. (2007). The cluster technique constructs a mixture of quadratic regression models, which are used to fit the geographical shape of TC tracks. Finite mixture models are able to fit highly non-Gaussian probability density functions using few component probability distribution functions. The model is fit to the data by maximizing the likelihood of the parameters conditioned on the data. One important

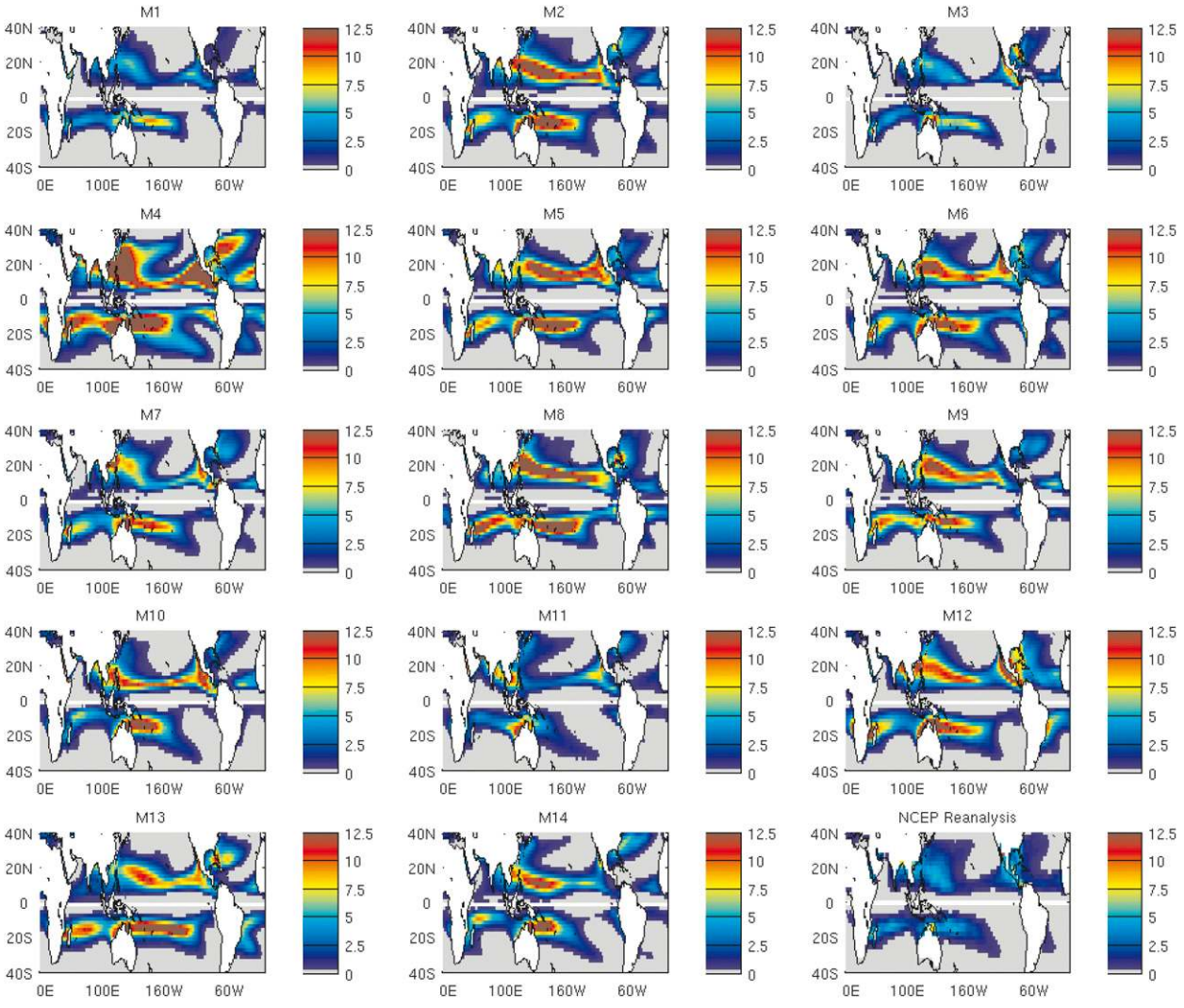

FIG. 4. Seasonal climatological genesis potential index in the models and the NCEP reanalysis for the period 1971–2000. The Northern (Southern) Hemisphere show the GPI seasonal mean for the August–October (ASO) [January–March (JFM)] season.

advantage of this method is that it easily accommodates tracks of different lengths. Each TC track is assigned to one of the clusters. The number of clusters to be used is not uniquely determined; the optimal choice depends on the log-likelihood values (interpreted as goodness of fit) and within-cluster spread (distance of all tracks in the cluster from the mean regression track). As the number of clusters K increase, the log-likelihood values increase and the within-cluster spread decreases, but both curves show diminishing improvement in fit for K higher than a certain value, which leads to an optimal range of K choices. The final selection within this range is usually based on the knowledge of the system. This technique has been applied to observed TC tracks in various regions, including the western North Pacific (Camargo et al. 2007c,d), the eastern North Pacific (Camargo et al. 2008), the Fiji Islands (Chand and Walsh 2009, 2010), the North Atlantic (Kossin et al. 2010), and more recently the Southern Hemisphere (Ramsay et al. 2012).

3. Historical and future global TC activity

Models tracks and first position locations in the eight models for the period 1980–2005 are shown in Figs. 1 and 2, respectively. Only one ensemble member is shown for models with more than one ensemble member. The models present a wide range of global TC activity. A few models (CCSM4, INM-CM4.0, and NorESM1-M) have very few TC tracks overall. Some models are relatively active in the South Pacific: for example, CanESM2, CSIRO Mk3.6.0, and HadGEM2-ES. A few other models have

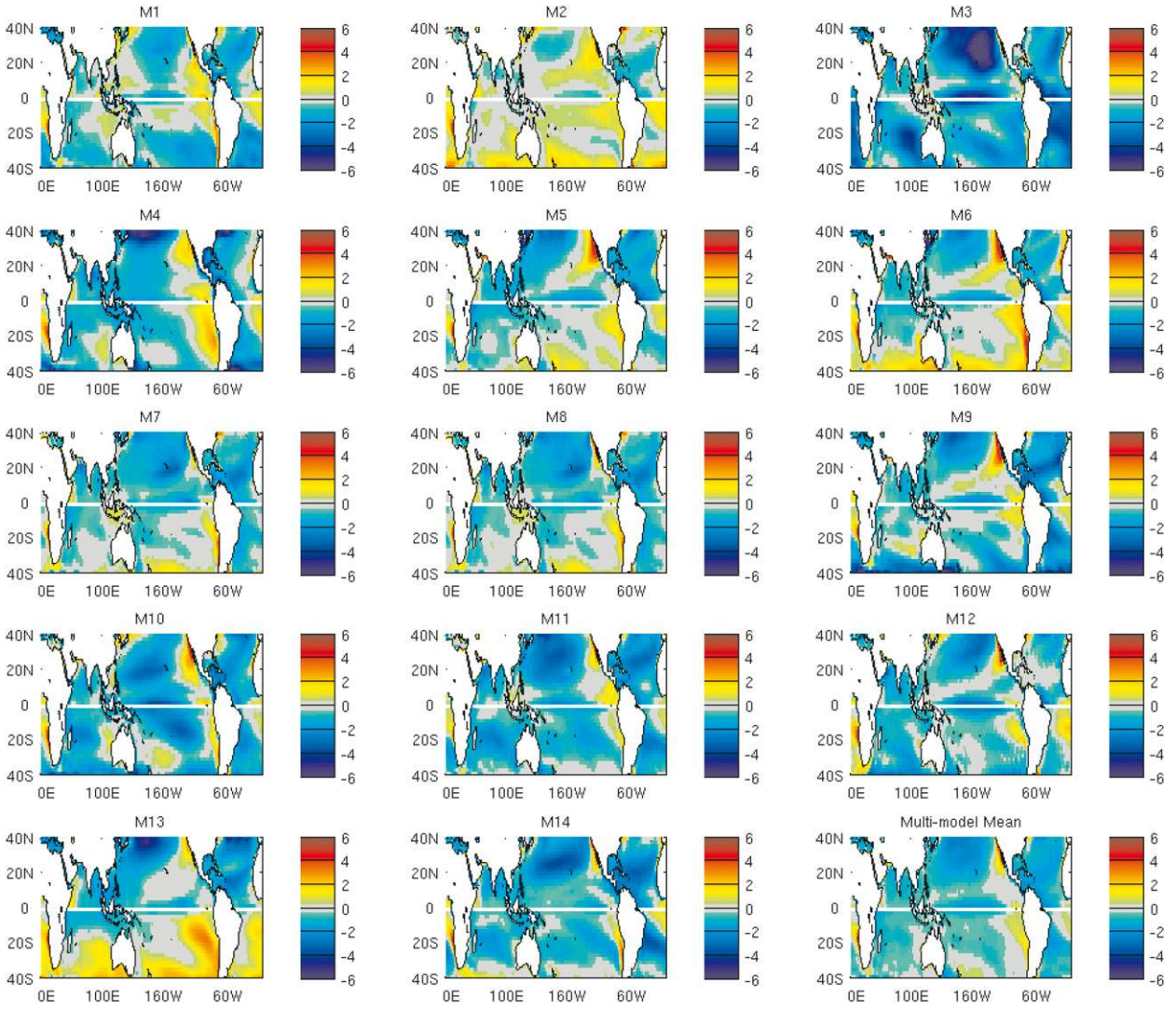

FIG. 5. Difference of SST in the models and Reynolds SST for the period 1971–2000. The Northern (Southern) Hemisphere show the GPI seasonal mean for the ASO (JFM) season.

few TCs in some basins but almost none in others (e.g., CCSM4, IPSL-CM5A-LR, and MIROC-ESM).

The models with the highest level of TC activity are CanESM2, CSIRO Mk3.6.0, GFDL CM3, GFDL-ESM2M, HadGEM2-ES, MIROC5, and MPI-ESM-LR, but there are significant differences among these models and all models have biases compared with observations. Both GFDL models are very active in the Pacific and Indian Oceans, with relatively fewer storms in the North Atlantic. Another interesting characteristic of the GFDL models is that TCs occur very close to the equator in the central and western Pacific and Indian Oceans but not in the eastern Pacific and North Atlantic. MRI-CGCM3is the most active model globally.

There are very few North Atlantic storms in the CanESM2, CSIRO Mk3.6.0, FGOALS-g2, and HadGEM2-ES models, with most TC activity occurring in the Southern Hemisphere, western North Pacific, and Bay of Bengal. The low production of TCs in the North Atlantic is a common issue among low-resolution models (see, e.g., Camargo et al. 2005), and many models have problems simulating well the TC activity in the North Atlantic, even if they are active in the western Pacific and Indian Oceans. There a few possible reasons for this problem: one is that the North Atlantic is marginal regarding the formation of storms and, therefore, minor model biases can easily lead to a reduction of the TC activity in the region. Furthermore, the production of the model storm is strongly related to the model easterly waves activity, and very often these waves are not well represented in the climate models. Similarly, the eastern North Pacific is commonly underactive, which has been related to easterly waves not

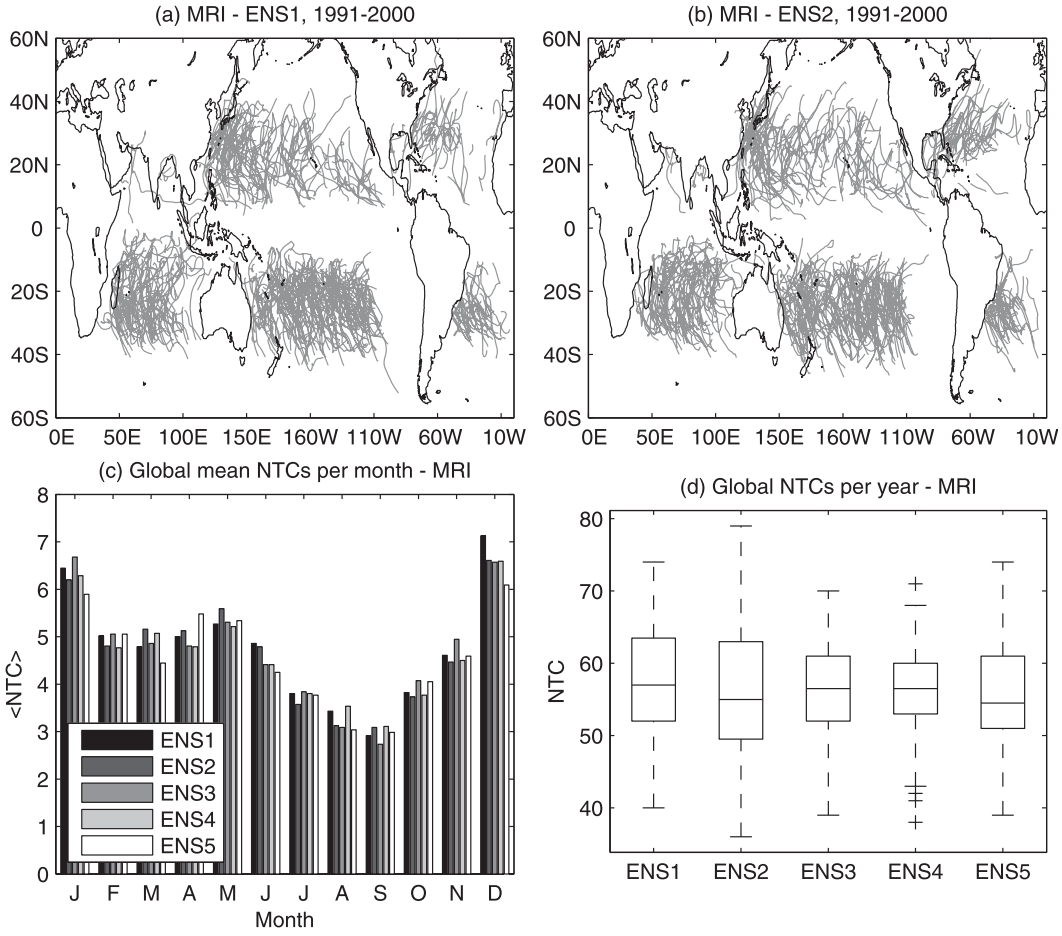

FIG. 6. Global tracks of the MPI-ESM-LR TCs for (a) ensemble member 1 (ENS1) and (b) ENS2. (c) Mean MPI-ESM-LR global NTC per month for five ensemble members (ENS1, ENS2, ENS3, ENS4, and ENS5) in the period 1950–2005. (d) Distributions of MPI-ESM-LR global NTC per year for three ensemble members in the period 1950–2005. Range boxes as in Fig. 3.

crossing into that basin from the Atlantic, as well as a poor representation of the Central America mountains in low-resolution models.

Some models tend to have very long tracks in the Southern Hemisphere (e.g., CanESM2, CSIRO Mk3.6.0, GFDL CM3, GFDL-ESM2), leading to a high level of TC activity more poleward than in observations. Here we only show storms with genesis in the tropical band (30°S–30°N). The frequency of storms forming in the subtropics and extratropics (not shown) has large differences among models. One possible explanation for this behavior is that the tracking scheme is not distinguishing well between tropical and extratropical storms for those specific models, despite one of the criteria being that the storm has a warm core, a common issue among tracking schemes (e.g., Horn et al. 2013). However, as this high-level activity out of the tropics only occurs in a few models, this issue needs to be examined further in more detail. Preliminary diagnosis of this issue was performed, but no clear solution was found.

The distribution of the global number of TCs per year in the period 1980–2005 in the models and in observations is given in Fig. 3. Typical of low-resolution climate models (Camargo et al. 2005, 2007e), all models have too few storms per year. There is not a clear relationship between model horizontal resolution and TC activity level, but the model with highest horizontal resolution (MRI-CGCM3, see Table 1) is the most active and closest to observed values. However, resolution does not completely explain TC activity level. For instance, CCSM4 has a similar resolution to MRI-CGCM3 but is very inactive and the GFDL models have a lower resolution than MPI-ESM-LR (Table 1) but their global TC activity levels are quite similar.

Comparison with the TC activity in the CMIP3 models (Meehl et al. 2007) is discouraging, with little

improvement in the CMIP5 model simulations of TC activity (Walsh et al. 2010, 2013). TC activity was seen to be better in CMIP3 models with higher horizontal resolution. Simulated TC frequency increases with increasing resolution if all other factors are kept constant in many cases (Bengtsson et al. 1995; Murakami and Sugi 2010), but not always (Strachan et al. 2013). However, model resolution is clearly not the only factor responsible for the quality of the TC simulations. TC frequency and spatial distribution in climate models are sensitive to changes in model convection schemes (Vitart et al. 2001; Kim et al. 2012; Reed and Jablonowski 2011a; Zhao et al. 2012). Walsh et al. (2013) pointed to dramatic changes in model TC frequency in two versions of the CMIP3 GFDL model with different dynamical cores and the same convection parameterizations. An extensive analysis of idealized simulations using different dynamical cores for the same model showed that the quality of the TC simulation was dependent on the interaction of the different model dynamical cores and moist convection parameterizations (Reed and Jablonowski 2012). In summary, increasing model horizontal resolution is not sufficient to improve its simulation of TC frequency, as the model TC activity is sensitive to physical parameterizations and dynamical cores.

A few models (MIROC5, MPI-ESM-LR, and MRI-CGCM3) are very active in the South Atlantic basin, a region where very few storms occur in observations. Hurricane Catarina (2004) was a very unusual event (Pezza and Simmonds 2005; McTaggart-Cowan et al. 2006). The occurrence of South Atlantic hurricanes in climate models is not unusual (e.g., Gualdi et al. 2008), but the level of activity in the MPI-ESM-LR and MRI-CGCM3 models in that region is quite high.

The climatological mean GPI is shown in Fig. 4 for all models and the NCEP reanalysis for the period 1971–2000. There is a large spread in the values of GPI among the models, as well as a variety of climatological patterns. As noted in previous studies (Camargo et al. 2007e; Tippett et al. 2011; Walsh et al. 2010, 2013), the GPI values in the models are much higher than in the reanalysis. These studies attributed the difference to the lower values of relative humidity in mid levels in the reanalysis compared to the climate models, as there are known differences between the relative humidity in the 40-yr European Centre for Medium-Range Weather Forecasts Re-Analysis (ERA) and NCEP reanalysis (Daoud et al. 2009) and biases in the midtroposphere relative humidity in the NCEP reanalysis (Bony et al. 1997). We calculated the difference between the models and NCEP reanalysis for the annual zonal-mean climatological relative humidity at 600 hPa between 40°S and 40°N for the period 1950–2005, and all models, with

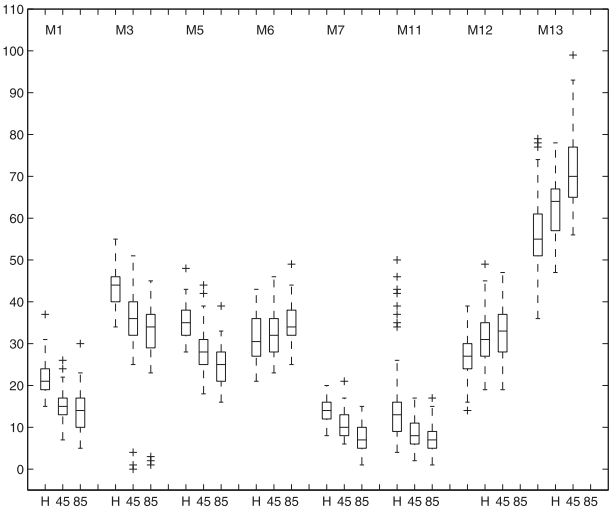

FIG. 7. Global number of TCs per year in models for the historical (H) run for the period 1951–2000 and in the future scenarios RCP4.5 (45) and RCP8.5 (85) in 2051–2100. Range boxes as in Fig. 3.

exception of CanESM2, have larger values than the reanalysis. Note that CanESM2 is the model with the smallest values of GPI.

One aspect of interest is the relationship between GPI and the TC occurrence in models. Low-resolution climate models tend to have more realistic patterns of GPI than of TC occurrence and there is no good relationship between GPI and TC occurrence in the models (Camargo et al. 2007e; Walsh et al. 2013). The same is true here: for instance, while CCSM4, INM-CM4.0, and NorESM1-M have very few TC geneses in the tropics and a very different pattern than observations, their GPI pattern is quite similar to the reanalysis. MRI-CGCM3, the model with the highest resolution, shows the best agreement between GPI and TC frequency, which is in agreement with Walsh et al. (2013). Even in the South Atlantic this relationship holds, with the MRI-CGCM3 GPI in that region being quite high and the model producing many TCs.

Figure 5 shows the difference between model SST and the NOAA observed SST for the period 1971–2000. In most models, the SST is colder than observations and this cold SST bias could potentially help to explain the low number of storms. It interesting to note that the MRI-CGCM3 SST is too warm in the Southern Hemisphere, where the model's GPI is high and the model produces too many TCs. A few models have warm SST anomalies in the western boundaries of the American continent. Various studies showed that future TC projections are sensitive to the specific SST patterns in the models (VS07b; Sugi et al. 2009; Villarini et al. 2011). However, similar to GPI, the direct relationship of TC

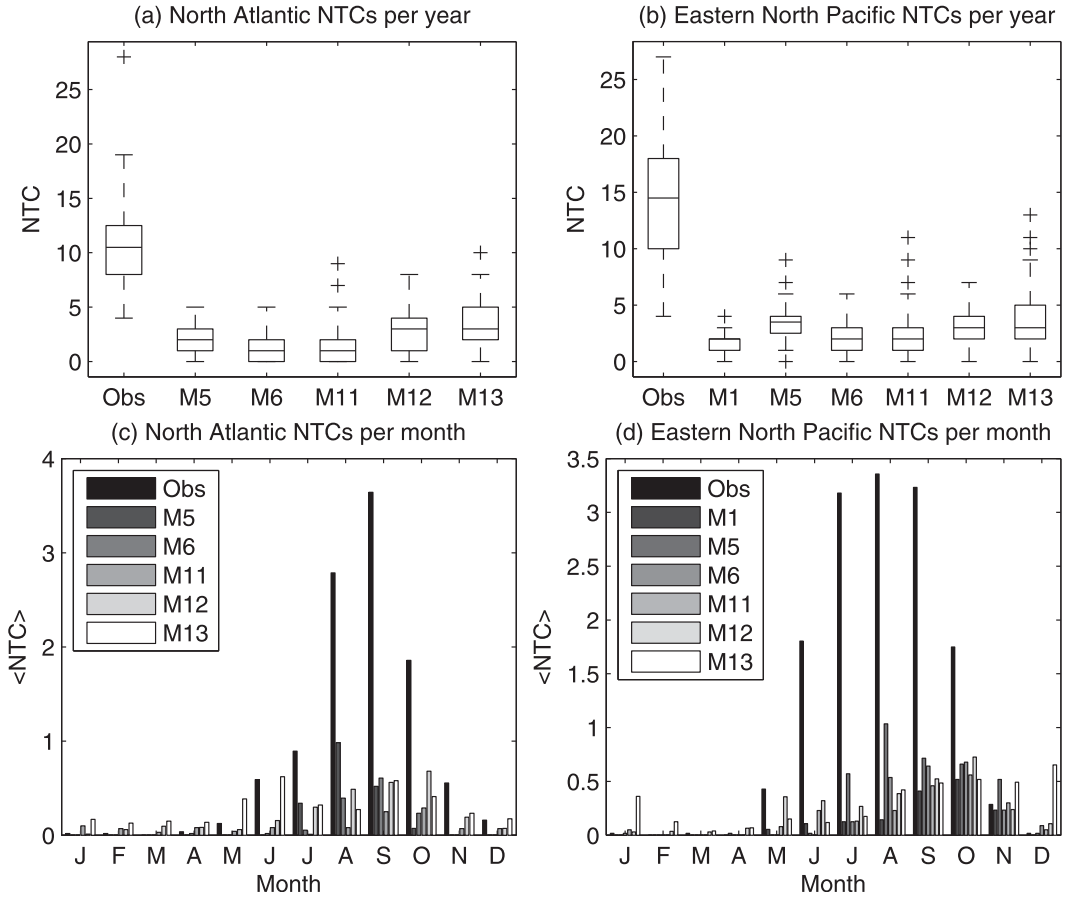

FIG. 8. (top) Distribution of the NTC in North Atlantic and eastern North Pacific in the period 1950–2005 for models and observation per year and (bottom) mean NTC per month. Range boxes as in Fig. 3.

frequency and SST bias is not enough to explain the differences among models in TC activity.

One point of interest is the variability of global TC activity between different ensemble members of the same model. Figure 6 shows the global tracks of two ensemble members of MRI-CGCM3, as well as the mean number of TCs (NTC) per month and the spread of the NTC per year for the five ensemble members. There is a clear similarity of the global tracks and NTC characteristics among the ensemble members of MRI-CGCM3. This result is in agreement with the assessment of ensemble member uncertainty in TC activity of Reed and Jablonowski (2011b), which concluded that the dominant differences were due to different model versions and resolutions and not due to internal variability.

Next we want to examine the model projections of global TC frequency in the twenty-first century. Here we exclude from our analysis the six models with mean NTC closest to zero globally (see Fig. 3). The distributions of global NTC per year in the historical runs and the two projection scenarios (RCP4.5 and RCP8.5) are shown in Fig. 7. There is little consistency among the models. While there is a slight increase in NTC in the future for the GFDL-ESM2M (M6) and MPI-ESM-LR (M12) models, there is a large increase in MRI-CGCM3 (M13) and a small decrease for the CanESM2 (M1), CSIRO Mk3.6.0 (M3), GFDL CM3 (M5), HadGEM2-ES (M7), and MIROC5 (M11) models. Knutson et al. (2010) analyzed the projections of global TC frequency in many high-resolution climate models, and the robust response among them was a small (but significant) decrease in the global frequency of TCs at the end of the twenty-first century. The lack of consistency among the models can be partly explained by the low resolution and bias in NTC in the models analyzed here. Recent results using a downscaling technique for the CMIP5 models (Emanuel 2013) resulted in an increase in global TC frequency in the twenty-first century.

In the case of MRI-CGCM3, the model with highest resolution in this set of CMIP5 models, the horizontal resolution is the same (120 km) as the lowest resolution model in Knutson et al. (2010). It is interesting that here

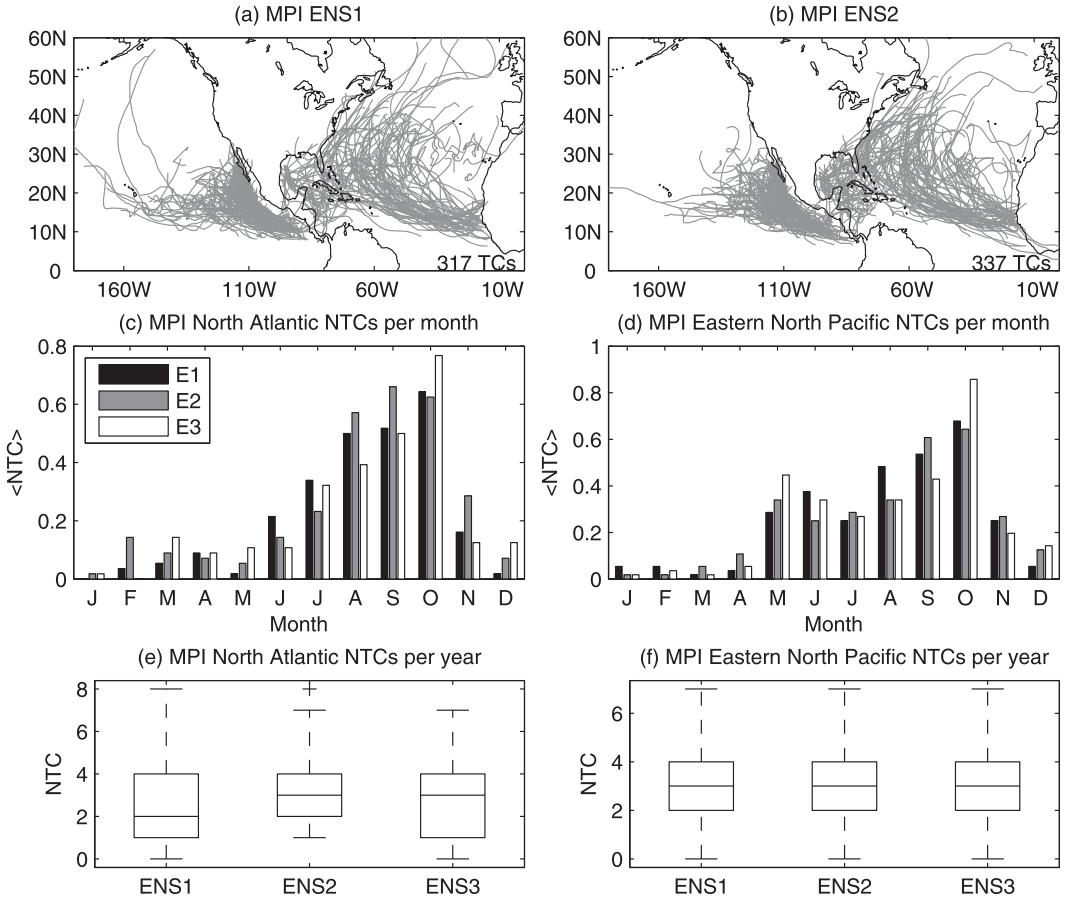

FIG. 9. Tracks of the MPI-ESM-LR TCs for (a) ensemble members (a) ENS1 and (b) ENS2 and the mean MPI-ESM-LR NTC per month in the (c) North Atlantic and (d) eastern North Pacific for three ensemble members (E1, E2, and E3) in the period 1950–2005. Distributions of MPI-ESM-LR NTC per year for three ensemble members in (e) the North Atlantic and (f) the eastern North Pacific in the period 1950–2005. Range boxes as in Fig. 3.

MRI-CGCM3 (Mizuta et al. 2012) projects an increase the frequency of TCs in the future, while previous results with the various versions of this atmospheric model projected a decrease in the global frequency of TCs when forced with fixed SSTs (Sugi et al. 2009, 2012; Murakami et al. 2012a,b), even for simulations with the same resolution that MRI-CGCM3 has in the CMIP5 (Murakami and Sugi 2010). The reasons for the differences in these results could have multiple sources: coupled ocean instead of fixed SSTs, coupling with chemical and carbon models, and differences in the algorithm used for detection and tracking TCs (including thresholds definitions; e.g., Walsh et al. 2007); however, in the case of this particular model, resolution is not one of the possible reasons for the differences. Similarly, the MPI-ESM-LR projections for an increase in global NTC, though not as dramatic as in the case of MRI-CGCM3, are still in contrast with results with previous projections using a high-resolution version of the model (Bengtsson et al. 2007b). It is particularly interesting that the two GFDL models have opposite projections for the future, but the differences between future and present projections are quite small in both cases.

4. TC activity in the North Atlantic and eastern North Pacific

We explore now in more detail the TC characteristics of these simulations in the North Atlantic (NATL) and the eastern North Pacific (ENP). Previous studies have shown that most low-resolution models have difficulty in simulating the mean NTC in those regions, even when they are able to simulate well the interannual variability (Bengtsson et al. 1995; Vitart et al. 1997; Camargo et al. 2005, 2007a; Walsh et al. 2010).

Projections of NATL TC activity have been the focus of many studies using high-resolution global climate models (Zhao et al. 2009), regional climate models (Knutson et al.

2008, 2013; Bender et al. 2010), and statistical–dynamical downscaling (Emanuel et al. 2008). We would like to examine if the CMIP5 model regional projection of the Atlantic TC activity is robust and if it is in agreement with these studies. Recently, Villarini and Vecchi (2012) used a statistical downscaling methodology to examine the twenty-first-century projections of Atlantic storms using the CMIP5 models. They obtained an increase in the number of TCs in the first half of the twenty-first century but obtained ambiguous results when the whole twenty-first century was considered. In the case of the ENP, there is no robust signal among models for that region (e.g., Emanuel et al. 2008).

The average NTC per month in the NATL and ENP in models and observations is shown in Fig. 8 for five and six models, respectively. In both basins all models have too few TCs per year; note that the other models (see Fig. 1) have even fewer storms or almost none. Examination of the annual cycle reveals that the models produce too few TCs during the active season and, in contrast, too many TCs during the inactive season when there are none or very few TCs in observations.

Figure 9 shows the tracks for two ensemble members of MPI-ESM-LR and the NTC distribution per year and the mean NTC per month for three MPI-ESM-LR ensemble members in the historical runs. Similar to global case for MRI-CGCM3, it is clear that, though there is variability in number and track patterns among the ensemble members of the same model for specific regions, these are much more similar to each other than to other models.

We now compare present TC activity with RCP4.5 and RCP8.5 projections of TC activity in the Atlantic and ENP. Figure 10 shows the distribution of TCs per year in the models in the present and future. There is no robust signal across models in changes of Atlantic NTC by the end of the twenty-first century. This result is not completely unexpected given the differences in the NTC climatology in the Atlantic in the models analyzed here. Furthermore, using a statistical downscaling technique, no robust changes in Atlantic NTC for the end of the twenty-first century were obtained either (Villarini and Vecchi 2012). However, dynamical downscaling points toward a decrease in the number of storms in the Atlantic for the CMIP5 and CMIP3 models (Knutson et al. 2013). Similar to the Atlantic, there is no robust change in the ENP NTC across the models.

Another aspect of TC activity that we would like to investigate is the possibility of track changes in the Atlantic. Given that TC landfall location is determined by its track, if there are significant changes in track types, these could lead to significant changes in landfall frequency and location. As an example, we apply cluster

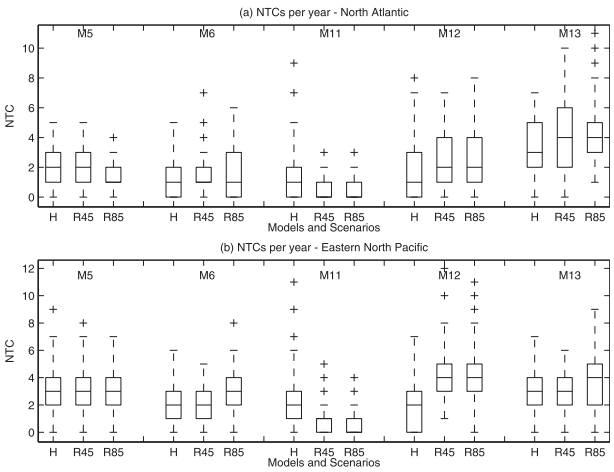

FIG. 10. NTC per year in the models in (top) the North Atlantic and (bottom) the eastern North Pacific for the historical (H) period 1951–2000 and RCP4.5 (R45) and RCP8.5 (R85) future scenarios (2051–2100). Range boxes as in Fig. 3.

analysis to the MPI-ESM-LR and MRI-CGCM3 models in the Atlantic, as these models have more ensemble members available and the track patterns of these models are not completely unrealistic. With cluster analysis, we separate the TC tracks into groups with similar track types (Fig. 11) and compare the model track types with the observed ones, as well as between models, identifying model biases and possible track shifts in the future climates.

We used all of the tracks in all scenarios and ensembles members to construct our cluster analysis. Details of the methodology can be found in Camargo et al. (2007e, 2008) and Kossin et al. (2010). Figure 11 shows the result of the cluster analysis for the MPI-ESM-LR (left panels) and MRI-CGCM3 (right panels) Atlantic tracks. The optimal number of cluster choice for observed tracks was $K = 4$ (Kossin et al. 2010). Here we use the same number of clusters. The four clusters in observations include a cluster of subtropical storms, one of Gulf of Mexico storms, and two types of deep tropics storms, one with formation more to the east of the basin and the other near the Caribbean islands (see Fig. 1 in Kossin et al. 2010).

MPI-ESM-LR has four clusters in the Atlantic that are similar to the observed, but the formation in the deep tropics near the Caribbean is weak (Fig. 11). The main difference in MRI-CGCM3 tracks and the observations is the existence of one additional subtropical cluster, with no correspondence to the observations, in the eastern Atlantic (Fig. 11h) and lack of formation in the deep tropics (Fig. 11f).

Analyzing the differences of cluster assignment of tracks between the historical and future scenarios of

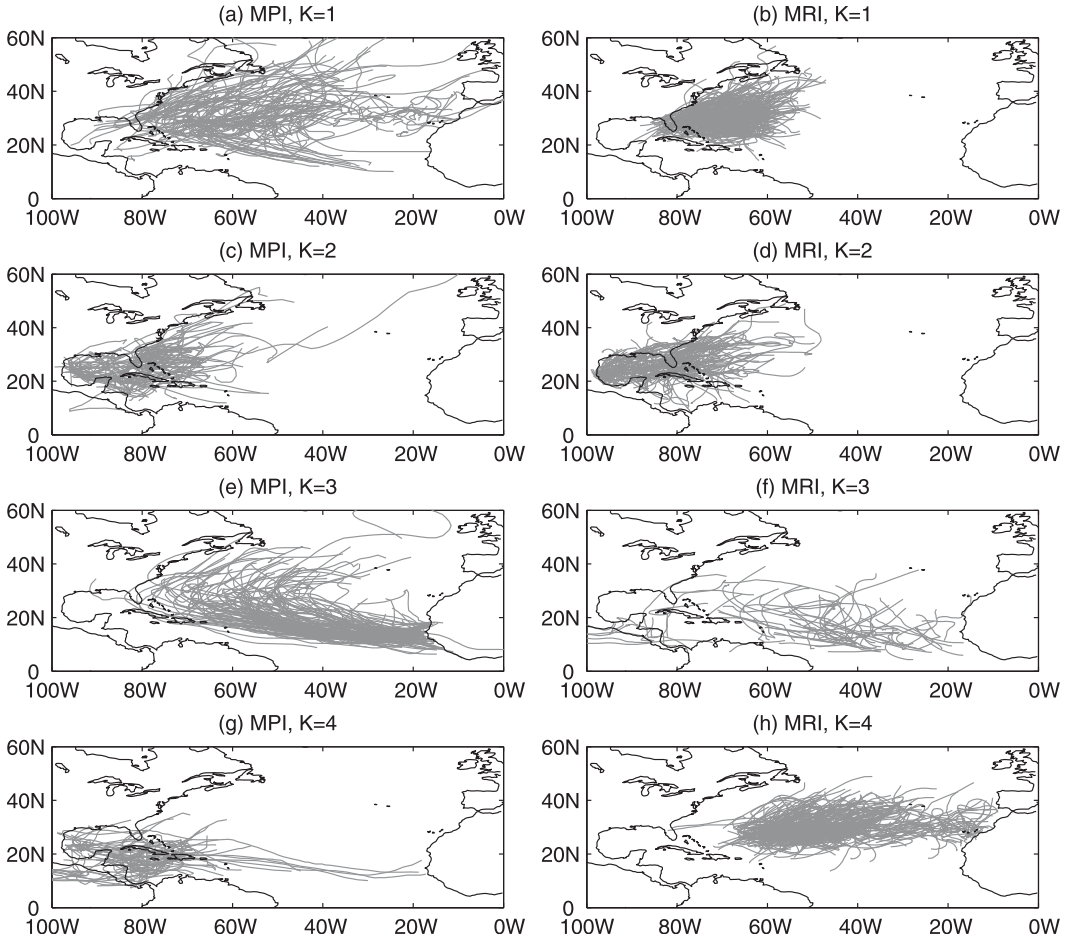

FIG. 11. North Atlantic TCs tracks by cluster (K1 to K4) for the (left) MPI-ESM-LR and (right) MRI-CGCM3 models. Tracks for one ensemble member of the historical, RCP4.5, and RCP8.5 runs are shown together for each cluster and model.

MPI-ESM-LR, there is a statistically significant increase in the percentage of storms in the subtropical cluster ($K = 2$) and a decrease in the percentage of storms in the tropical cluster ($K = 1$). In the case of MRI-CGCM3, there is an increase in the Gulf of Mexico storms and a decrease in the subtropical storms: namely, $K = 1$ and $K = 4$, the latter having no counterpart in the observations.

The Atlantic tracks in the high-resolution version of MRI-CGCM3 used in Murakami and Wang (2010) are much more similar to the observed Atlantic tracks. There are no western Atlantic subtropical tracks, as seen here. Murakami and Wang (2010) examined possible changes in NATL storms using high-resolution simulations of MRI-CGCM3 and found significant zonal track changes with a decrease (increase) of TC occurrence in the western (eastern) part of the basin. They attributed these track changes to changes in genesis locations, not to changes in circulation. Colbert et al. (2013) used the winds of the CMIP3 models to obtain Atlantic TC tracks simulated by a beta advection model. They obtained a statistically decrease in straight-moving tracks (westward) and an increase in the recurving tracks in the twenty-first century, which could also be viewed as a west–east zonal shift.

5. Changes in the large-scale environment

Given that TC activity in most CMIP5 models is still not realistic, it is important to use an alternative approach to infer future changes in TC activity. We expect that the CMIP5 models are better able to simulate changes in the large-scale environment than the TCs themselves. Although the large-scale environmental fields are not very good predictors of the TC model frequency in specific regions in the CMIP5 models, we expect that they will relate well to the TCs in the real world. Therefore, we will now examine changes in the large-scale environment in the RCP8.5 scenario, compared with the historical

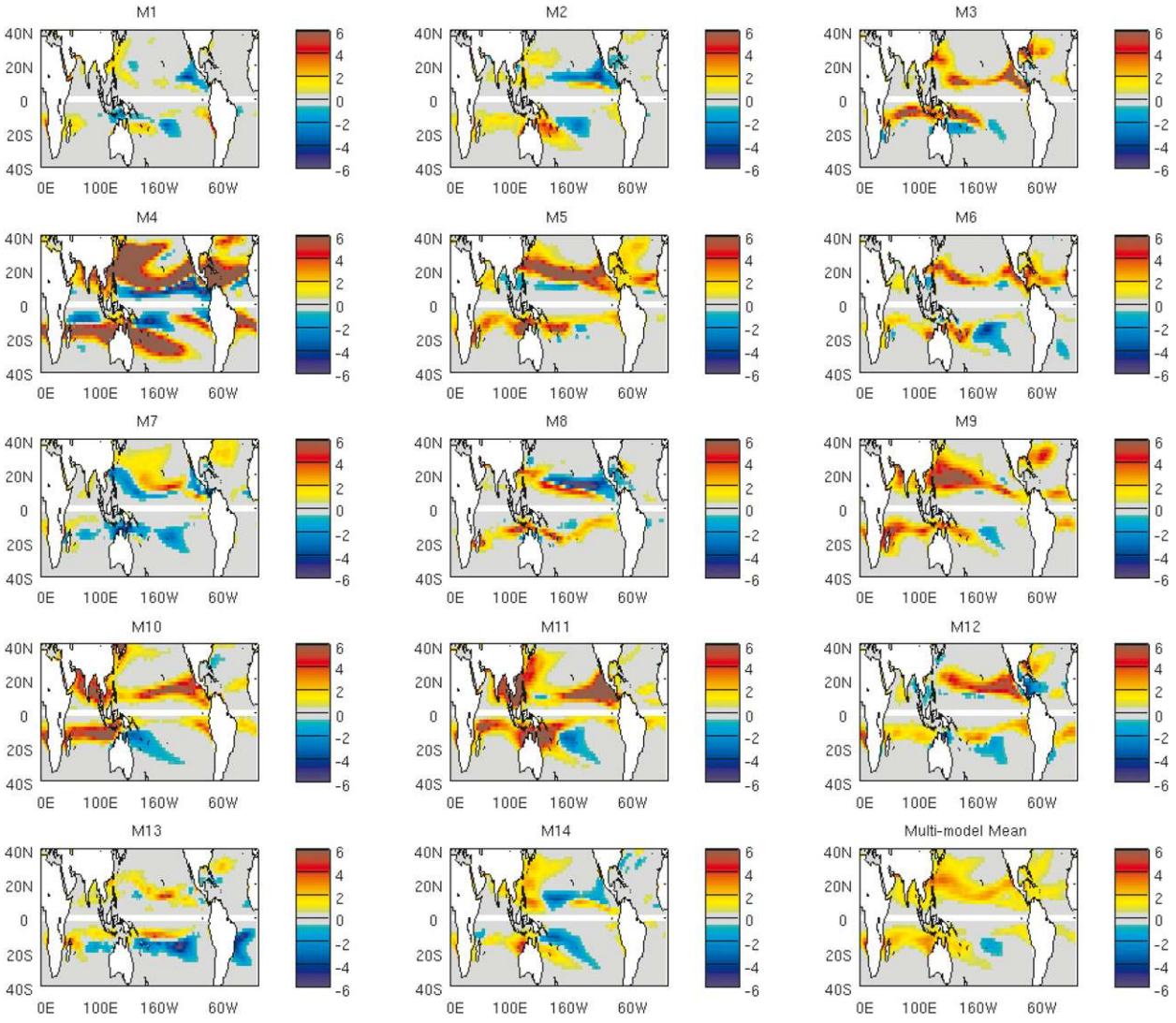

FIG. 12. Difference of model GPI climatology between the RCP8.5 future scenario (2071–2100) and historical (1971–2000) simulation. The multimodel mean difference is shown in the bottom right panel. In all panels, the difference in ASO (JFM) is shown in the Northern (Southern) Hemisphere. All ensemble members available are used to calculate the GPI climatology per model and scenario.

simulations in all models. In Fig. 12 we show the difference in the climatological genesis potential index in the future and present for all models and the multimodel mean. The climatological GPI in the historical simulation for the same models was shown in Fig. 4. The model mean GPI difference is positive in most regions, with the exception of the central south Pacific. An increase in the GPI in the future can be interpreted as an increase in the global TC frequency in these models in a future climate. However, in some cases model GPI is observed to increase even when the model frequency decreases (Camargo et al. 2012), therefore we need caution in interpreting this result. For instance, the model with the largest increase of GPI is the MIROC5 (M11), which has a decrease in the number of TCs globally in this scenario (Fig. 5) as well. In some models, the GPI difference patterns are shifts in location, such as in the Southern Hemisphere (M2, M3, M4, M13, and M14) and western North Pacific (M2, M4, M7, M8, and M14). These shifts resemble GPI ENSO difference patterns (El Niño minus La Niña), discussed in Camargo et al. (2007a). Another interesting feature is the decrease of GPI in the MRI-CGCM3 (M13) in the South Atlantic, where there is an unrealistically high number of TCs in the historical run (Fig. 1g). It is important to note that Emanuel (2013) obtained an increase in a genesis index (Emanuel 2010) at the end twenty-first century for the CMIP5 models, as well as an increase in the global frequency of TCs at the

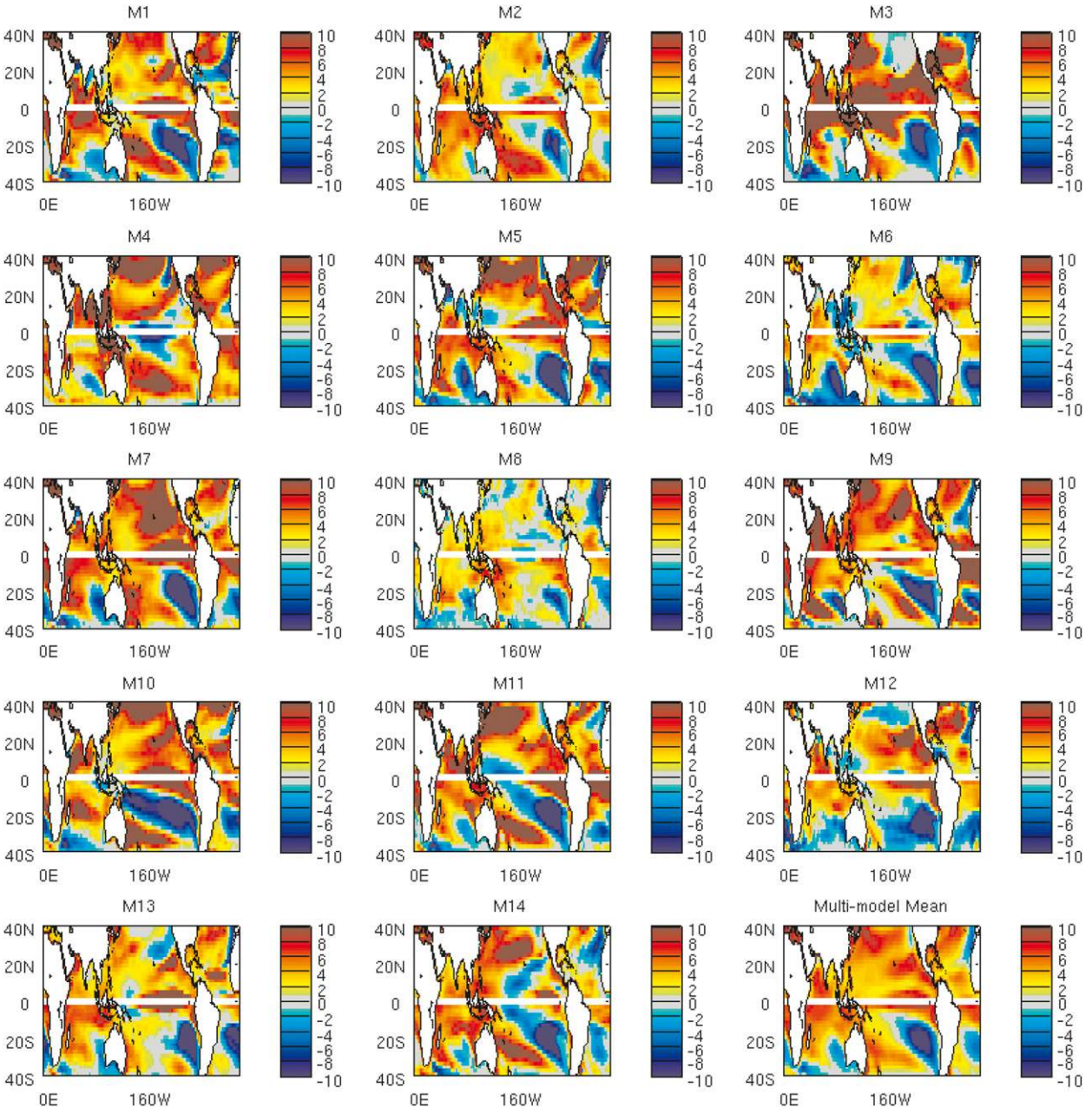

FIG. 13. As in Fig. 12, but of potential intensity.

end of twenty-first century when downscaling the CMIP5 models.

VS07a calculated the model mean difference of GPI in future and present climates for the CMIP3 models in the June–November period (Fig. 4d in VS07a). In that case, there was also an increase in most of the Northern Hemisphere GPI in the ensemble mean with a maximum in the western North Pacific, with exception of the ENP where the GPI decreased. Here the model mean difference is positive in the whole Northern Hemisphere.

Another quantity of interest is the potential intensity, which is the theoretical maximum of TCs. Figure 13 shows the difference of the potential intensity in the RCP8.5 and historical scenarios for the individual models and model mean. The PI increases in most of the Northern Hemisphere in all models, with exception of a small region of the eastern part of the NATL and Pacific Oceans. In some models, the decrease in PI in the NATL is restricted to a small region near Africa, while in other models a larger region in the NATL has negative PI differences, including

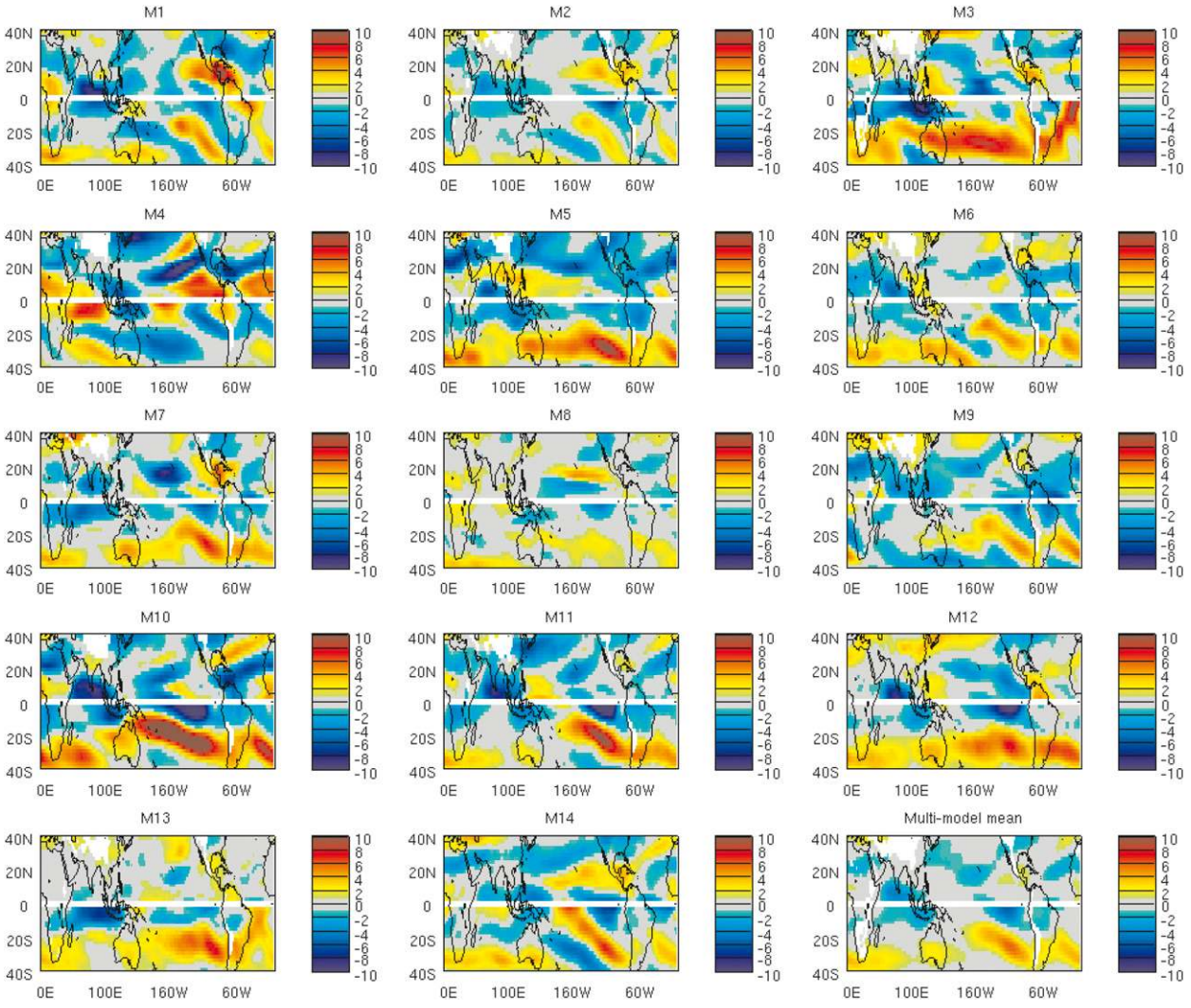

FIG. 14. As in Fig. 12, but of climatological model vertical wind shear. The vertical wind shear magnitude is calculated as the magnitude of the difference between the 200- and 850-hPa winds.

the Gulf of Mexico and MDR region. In the Southern Hemisphere, there is an increase in PI in most regions. In all models there is a strong decrease in PI in the southeast Pacific and Atlantic, regions where normally TCs do not occur. The VS07a and VS07b analysis of the PI of the CMIP3 models for the June–November season has a very similar pattern in the Northern Hemisphere to that shown here: an increase in PI in most of the Northern Hemisphere, with one maximum near Hawaii and the other centered on the equator near the date line, and a decrease in PI in the NATL, which was attributed to changes in the remote SST (VS07b). The NATL negative region in the CMIP5 model mean PI differences is smaller and more restricted to the eastern Atlantic than in the case of CMIP3.

We also analyzed changes in the magnitude of the vertical wind shear in future and present climates (Fig. 14). Most models have large regions of increased (decreased) vertical shear in the subtropical (tropical) latitudes of the Southern Hemisphere, which could lead to an equatorial shift of the TC activity in the Southern Hemisphere. In the Northern Hemisphere, many models show an increase in the vertical shear in the ENP and Caribbean region, extending in some cases into the Gulf of Mexico. In contrast, the eastern part of the Atlantic, western North Pacific, and northern Indian Ocean have a reduction of the vertical wind shear. Once more, the model mean pattern is extremely similar to that obtained in the CMIP3 models in VS07a for the Northern Hemisphere TC season. These changes in vertical shear are associated to the projected decrease in the Pacific Walker circulation (VS07a), while the near-equatorial vertical shear weakening was related to the near-equatorial zonal overturning

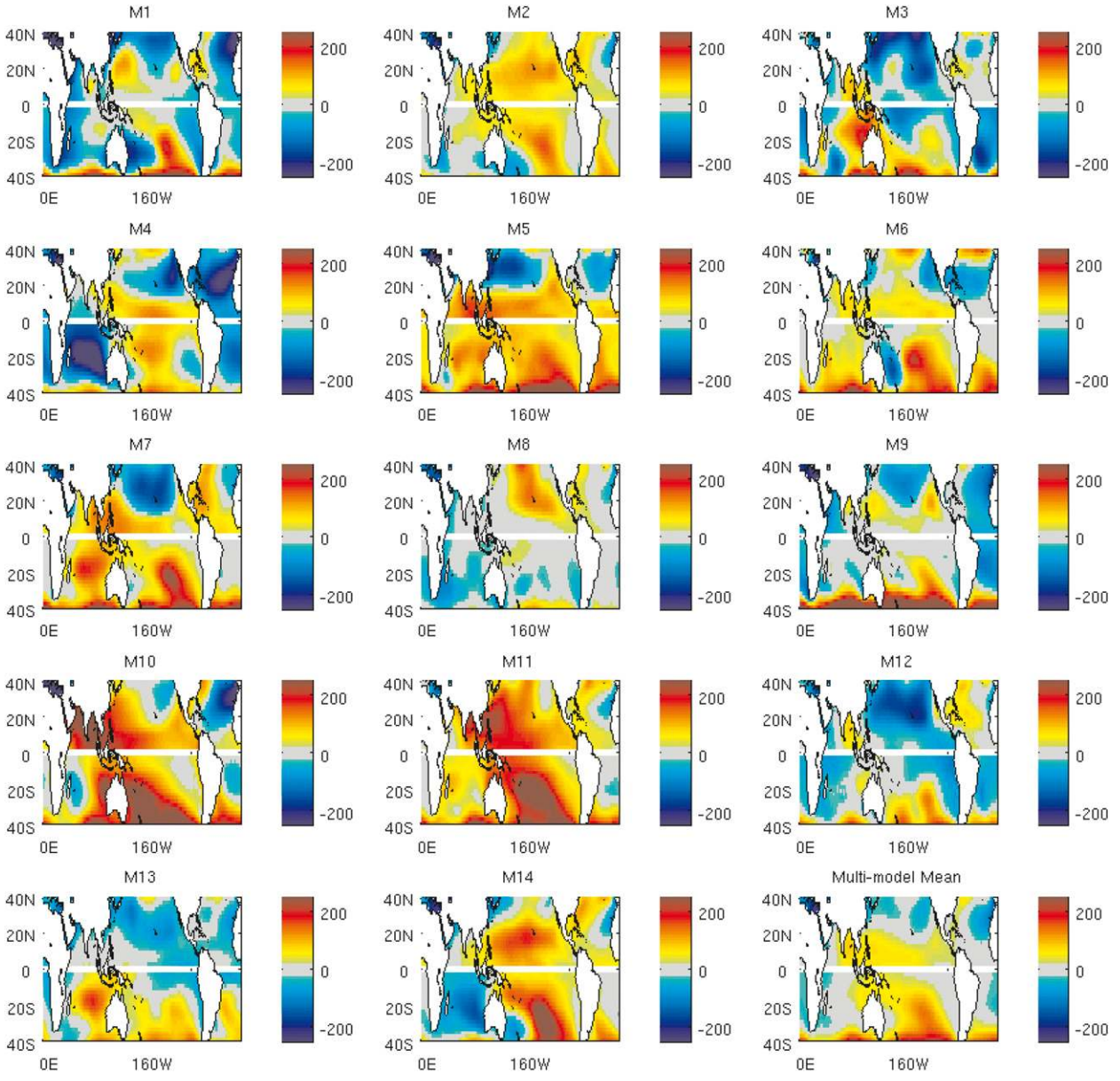

FIG. 15. As in Fig. 12, but of climatological sea level pressure.

(VS07a; Vecchi and Soden 2007c; Vecchi et al. 2006) due to global thermodynamic constraints (Held and Soden 2006).

The difference of sea level pressure (SLP) in the RCP8.5 and historical runs is shown in Fig. 15. The movement of TCs (i.e., their tracks) is largely determined by the ambient flow, or steering winds, with modifications due to the beta effect (Chan 2005). The steering winds are strongly related to the position and strength of the subtropical highs. Therefore, any future changes in the subtropical highs will be associated with shifts in TC tracks (Colbert and Soden 2012). The differences in SLP in the NATL shown in Fig. 15 for most models are associated with a westward expansion of the subtropical high, which could potentially lead to more landfalls in the southeast region of the United States. Li et al. (2013) has noticed this extension of the NATL subtropical high in the CMIP5 models for the RCP4.5 scenario and it was also present in the CMIP3 models (Li et al. 2011). In the western North Pacific, the increase in the SLP in the RCP8.5 projections could indicate a southwestward shift of the subtropical high. Similarly, the increase of SLP in

the Southern Hemisphere could be related to an equatorial shift of the subtropical high in the South Pacific and south Indian Ocean.

6. Summary

An assessment of the TC activity in eight CMIP5 models was presented. Although the typical model resolution increased since the previous CMIP3 assessment, model global TC frequency is still much lower than observed. Only in the model with the highest resolution is global TC occurrence near the observed value, but this number includes a high number of Southern Hemisphere TCs, some in regions with very low frequency in observations. Furthermore, there are still deficiencies in the geographical patterns of the TC tracks and formation, with many models being relatively active in the western North Pacific, Indian Ocean, and Southern Hemisphere and inactive in the North Atlantic and eastern North Pacific. There is no robust signal across the models in changes in global TC frequency for future scenarios. An analysis of the regional TC activity in the ENP and NATL did not detect any robust changes in TC frequency in those two regions either.

Given the current state of the art of the CMIP5 in generating model TC activity, it is fundamental to continue using different approaches to infer future TC activity. One way to do that is to examine the large-scale environmental variables projection changes associated with TC activity. The CMIP5 models projected large-scale environmental changes are very consistent with the CMIP3 results. These changes in the environmental fields in future projections will hopefully be related to TC activity in the future, even if they are not strongly related to the model TCs with low resolution. More detailed analysis of the environmental changes is necessary: for instance, the seasonality of PI, which had changes in the CMIP3 models (Sobel and Camargo 2011). As basinwide PI trends can be larger than actual local potential intensity (PI) trends (Kossin and Camargo 2009), caution must be taken not to overestimate future trends when using basinwide large-scale variables.

It is also important to continue using a variety of downscaling methods (statistical and dynamical) to infer future projections of TC frequency, intensity, and tracks (e.g., Knutson et al. 2008; Villarini and Vecchi 2012, 2013). High-resolution models forced with fixed SST from the CMIP5 models (e.g., Zhao et al. 2009) and statistical–dynamical downscaling results (e.g., Emanuel et al. 2008) should still give a better assessment of future track and frequency projections than one using low-resolution models.

The first studies that used downscaling techniques for the CMIP5 models have just been published. In Emanuel (2013) downscaling of the CMIP5 models led to an increase in the global TC frequency in the twenty-first century, contrasting a decrease in the global frequency of TCs at the end of twenty-first century obtained when downscaling the CMIP3 models with the same technique. A dynamical downscaling of the CMIP3 and CMIP5 model projections over the North Atlantic (Knutson et al. 2013) resulted in a significant reduction of TC frequency by the end of the twenty-first century and an increase in frequency of very intense storms (Categories 4 and 5), in agreement with previous results (Knutson et al. 2008; Bender et al. 2010).

Acknowledgments. SJC would like to thank Haibo Liu and Naomi Henderson for collecting, managing, and serving the CMIP5 data at the Lamont-Doherty Earth Observatory of Columbia University and Michael Tippett for suggestions on the manuscript. SJC is supported by the National Oceanic and Atmospheric Administration/Modeling Analysis and Prediction Program (MAPP) under Grant NA11OAR4310093 and is part of the NOAA/MAPP CMIP5 Task Force. We acknowledge the World Climate Research Programme's Working Group on Coupled Modelling, which is responsible for CMIP, and we thank the climate modeling groups (listed in Tables 1 and 2) for producing and making available their model output. For CMIP the U.S. Department of Energy Program for Climate Model Diagnosis and Intercomparison provides coordinating support and led development of software infrastructure in partnership with the Global Organization for Earth System Science Portals.

REFERENCES

Bao, Q., and Coauthors, 2013: The Flexible Global Ocean-Atmosphere-Land System model, spectral version: FGOALS-s2. *Adv. Atmos. Sci.,* **30,** 561–576.

Bender, M. A., T. R. Knutson, R. E. Tuleya, J. J. Sirutis, G. A. Vecchi, S. T. Garner, and I. M. Held, 2010: Modeled impact of anthropogenic warming on the frequency of intense Atlantic hurricanes. *Science,* **327,** 454–458.

Bengtsson, L., H. Böttger, and M. Kanamitsu, 1982: Simulation of hurricane-type vortices in a general circulation model. *Tellus,* **34,** 440–457.

——, M. Botzet, and M. Esch, 1995: Hurricane-type vortices in a general circulation model. *Tellus,* **47A,** 175–196.

——, K. I. Hodges, and M. Esch, 2007a: Tropical cyclones in a T159 resolution global climate model: Comparison with observations and re-analysis. *Tellus,* **59A,** 396–416.

——, ——, ——, N. Keenlyside, L. Kornblueh, J.-J. Luo, and T. Yamagata, 2007b: How many tropical cyclones change in a warmer climate? *Tellus,* **59A,** 539–561.

Bister, M., and K. A. Emanuel, 1998: Dissipative heating and hurricane intensity. *Meteor. Atmos. Phys.,* **65,** 223–240.

——, and ——, 2002a: Low frequency variability of tropical cyclone potential intensity: 1. Interannual to interdecadal variability. *J. Geophys. Res.,* **107,** 4801, doi:10.1029/2001JD000776.

——, and ——, 2002b: Low frequency variability of tropical cyclone potential intensity: 2. Climatology for 1982–1995. *J. Geophys. Res.,* **107,** 4621, doi:10.1029/2001JD000780.

Bony, S., Y. Sud, K. M. Lau, J. Susskind, and S. Saha, 1997: Comparison and satellite assessment of NASA/DAO and NCEP–NCAR reanalyses over tropical ocean: Atmospheric hydrology and radiation. *J. Climate,* **10,** 1441–1462.

Bruyère, C. L., G. J. Holland, and E. Towler, 2012: Investigating the use of a genesis potential index for tropical cyclones in the North Atlantic basin. *J. Climate,* **25,** 8611–8626.

Camargo, S. J., and S. E. Zebiak, 2002: Improving the detection and tracking of tropical cyclones in atmospheric general circulation models. *Wea. Forecasting,* **17,** 1152–1162.

——, and A. G. Barnston, 2009: Experimental seasonal dynamical forecasts of tropical cyclone activity at IRI. *Wea. Forecasting,* **24,** 472–491.

——, ——, and S. E. Zebiak, 2005: A statistical assessment of tropical cyclone activity in atmospheric general circulation models. *Tellus,* **57A,** 589–604.

——, K. A. Emanuel, and A. H. Sobel, 2007a: Use of a genesis potential index to diagnose ENSO effects on tropical cyclone genesis. *J. Climate,* **20,** 4819–4834.

——, H. Li, and L. Sun, 2007b: Feasibility study for downscaling seasonal tropical cyclone activity using the NCEP regional spectral model. *Int. J. Climatol.,* **27,** 311–325.

——, A. W. Robertson, S. J. Gaffney, P. Smyth, and M. Ghil, 2007c: Cluster analysis of typhoon tracks. Part I: General properties. *J. Climate,* **20,** 3635–3653.

——, ——, ——, ——, and ——, 2007d: Cluster analysis of typhoon tracks. Part II: Large-scale circulation and ENSO. *J. Climate,* **20,** 3654–3676.

——, A. H. Sobel, A. G. Barnston, and K. A. Emanuel, 2007e: Tropical cyclone genesis potential index in climate models. *Tellus,* **59A,** 428–443.

——, A. W. Robertson, A. G. Barnston, and M. Ghil, 2008: Clustering of eastern North Pacific tropical cyclone tracks: ENSO and MJO effects. *Geochem. Geophys. Geosyst.,* **9,** Q06V05, doi:10.1029/2007GC001861.

——, M. C. Wheeler, and A. H. Sobel, 2009: Diagnosis of the MJO modulation of tropical cyclogenesis using an empirical index. *J. Atmos. Sci.,* **66,** 3061–3074.

——, M. K. Tippett, A. H. Sobel, G. A. Vecchi, M. Zhao, and I. M. Held, 2012: Analysis of tropical cyclone genesis indices for climate change using the HIRAM model. Preprints, *30th Conf. on Hurricanes and Tropical Meteorology,* Ponte Vedra Beach, FL, Amer. Meteor. Soc., 4B.1. [Available online at https://ams.confex.com/ams/30Hurricane/webprogram/Paper205593.html.]

——, M. Ting, and Y. Kushnir, 2013: Influence of local and remote SST on North Atlantic potential intensity. *Climate Dyn.,* **40,** 1515–1529.

Chan, J. C. L., 2005: The physics of tropical cyclone motion. *Annu. Rev. Fluid Mech.,* **37,** 99–128.

Chand, S. S., and K. J. E. Walsh, 2009: Tropical cyclone activity in the Fiji region: Spatial patterns and relationship to large-scale circulation. *J. Climate,* **22,** 3877–3893.

——, and ——, 2010: The influence of the Madden–Julian oscillation on tropical cyclone activity in the Fiji region. *J. Climate,* **23,** 868–886.

Chauvin, F., J.-F. Royer, and M. Déqué, 2006: Response of hurricane-type vortices to global warming as simulated by ARPEGE-Climat at high resolution. *Climate Dyn.,* **27,** 377–399.

Chen, J.-H., and S.-J. Lin, 2011: The remarkable predictability of inter-annual variablity of Atlantic hurricanes during the past decade. *Geophys. Res. Lett.,* **38,** L11804, doi:10.1029/2011GL047629.

Chu, J.-H., C. R. Sampson, A. S. Levine, and E. Fukada, 2002: The Joint Typhoon Warming Center tropical cyclone best-tracks, 1945-2000. NRL Tech. Rep. NRL/MR/7540-02-16, 22 pp.

Colbert, A. J., and B. J. Soden, 2012: Climatological variations in North Atlantic tropical cyclone tracks. *J. Climate,* **25,** 657–673.

——, ——, G. A. Vecchi, and B. P. Kirtman, 2013: The impact of anthropogenic climate change on North Atlantic tropical cyclone tracks. *J. Climate,* **26,** 4088–4095.

Daoud, A. B., E. Sauquet, M. Langand, C. Obled, and G. Bontron, 2009: Comparison of 850-hPa relative humidity between ERA-40 and NCEP/NCAR re-analyses: Detection of suspicious data in ERA-40. *Atmos. Sci. Lett.,* **10,** 43–47.

Donner, L. J., and Coauthors, 2011: The dynamical core, physical parameterizations, and basic simulation characteristics of the atmospheric component of the GFDL global coupled model CM3. *J. Climate,* **24,** 3484–3519.

Emanuel, K. A., 1988: The maximum intensity of hurricanes. *J. Atmos. Sci.,* **45,** 1143–1155.

——, 1995: Sensitivity of tropical cyclones to surface exchange coefficients and a revised steady-state model incorporating eye dynamics. *J. Atmos. Sci.,* **52,** 3969–3976.

——, 2000: A statistical analysis of hurricane intensity. *Mon. Wea. Rev.,* **128,** 1139–1152.

——, 2010: Tropical cyclone activity downscaled from NOAA-CIRES reanalysis, 1908–1958. *J. Adv. Model. Earth Syst,* **2,** 1, doi:10.3894/JAMES.2010.2.1.

——, 2013: Downscaling CMIP5 climate models shows increased tropical cyclone activity over the 21st century. *Proc. Natl. Acad. Sci. USA,* **110,** 12 219–12 224, doi:10.1073/pnas.1301293110.

——, and D. S. Nolan, 2004: Tropical cyclone activity and the global climate system. Preprints, *26th Conf. on Hurricanes and Tropical Meteorology,* Miami, FL, Amer. Meteor. Soc., 10A.2. [Available online at http://ams.confex.com/ams/pdfpapers/75463.pdf.]

——, R. Sundararajan, and J. Williams, 2008: Hurricanes and global warming: Results from downscaling IPCC AR4 simulations. *Bull. Amer. Meteor. Soc.,* **89,** 347–367.

Gaffney, S. J., 2004: Probabilistic curve-aligned clustering and prediction with regression mixture models. Ph.D. dissertation, University of California, Irvine, 299 pp.

——, A. W. Robertson, P. Smyth, S. J. Camargo, and M. Ghil, 2007: Probabilistic clustering of extratropical cyclones using regression mixture models. *Climate Dyn.,* **29,** 434–440.

Gent, P. R., and Coauthors, 2011: The Community Climate System Model version 4. *J. Climate,* **24,** 4973–4991.

Gray, W. M., 1979: Hurricanes: Their formation, structure and likely role in the tropical circulation. *Meteorology over the Tropical Oceans,* D. B. Shaw, Ed., Royal Meteorological Society, 155–218.

Gualdi, S., E. Scoccimarro, and A. Navarra, 2008: Changes in tropical cyclone activity due to global warming: Results from a high-resolution coupled general circulation model. *J. Climate,* **21,** 5204–5228.

Held, I. M., and B. J. Soden, 2006: Robust responses of the hydrological cycle to global warming. *J. Climate,* **19,** 5686–5699.

Horn, M., K. Walsh, and A. Ballinger, 2013: Detection of tropical cyclones using a phenomenon-based cyclone tracking scheme. *Proc. U.S. CLIVAR Hurricane Workshop,* Princeton, NJ, Geophysical Fluid Dynamics Laboratory. [Available online at http://www.usclivar.org/sites/default/files/meetings/Walsh_clivar_gfdl_2013.pdf.]

Jarvinen, B. R., C. J. Neumann, and M. A. S. Davis, 1984: A tropical cyclone data tape for the North Atlantic basin, 1886-1983: Contents, limitations, and uses. NOAA Tech. Memo. NWS NHC 22, 21 pp.

Jiang, X., M. Zhao, and D. E. Waliser, 2012: Modulation of tropical cyclones over the eastern Pacific by intraseasonal variability simulated in an AGCM. *J. Climate,* **25,** 6524–6538.

Jones, C. D., and Coauthors, 2011: The HadGEM2-ES implementation of CMIP5 centennial simulations. *Geosci. Model Dev.,* **4,** 543–570.

Kalnay, E., and Coauthors, 1996: The NCEP/NCAR 40-Year Reanalysis Project. *Bull. Amer. Meteor. Soc.,* **77,** 437–471.

Kim, D., A. H. Sobel, A. D. del Genio, Y. Chen, S. J. Camargo, M.-S. Yao, M. Kelley, and L. Nazarenko, 2012: The tropical subseasonal variability simulated in the NASA GISS general circulation model. *J. Climate,* **25,** 4641–4659.

Kistler, R., and Coauthors, 2001: The NCEP–NCAR 50-Year Reanalysis: Monthly means CD-ROM and documentation. *Bull. Amer. Meteor. Soc.,* **82,** 247–267.

Knutson, T. R., J. J. Sirutis, S. T. Garner, G. A. Vecchi, and I. M. Held, 2008: Simulated reduction in Atlantic hurricane frequency under twenty-first-century warming conditions. *Nat. Geosci.,* **1,** 359–364.

——, and Coauthors, 2010: Tropical cyclones and climate change. *Nat. Geosci.,* **3,** 157–163.

——, and Coauthors, 2013: Dynamical downscaling projections of twenty-first-century Atlantic hurricane activity: CMIP3 and CMIP5 model-based scenarios. *J. Climate,* **26,** 6591–6617.

Korty, R. L., S. J. Camargo, and J. Galewsky, 2012a: Tropical cyclone genesis factors in simulations of the Last Glacial Maximum. *J. Climate,* **25,** 4348–4365.

——, ——, and ——, 2012b: Variations in tropical cyclone genesis factors in simulations of the Holocene epoch. *J. Climate,* **25,** 8196–8211.

Kossin, J. P., and S. J. Camargo, 2009: Hurricane track variability and secular potential intensity trends. *Climatic Change,* **9,** 329–337.

——, ——, and M. Sitkowski, 2010: Climate modulation of North Atlantic hurricane tracks. *J. Climate,* **23,** 3057–3076.

Landman, W. A., A. Seth, and S. J. Camargo, 2005: The effect of regional climate model domain choice on the simulation of tropical cyclone-like vortices in the southwestern Indian Ocean. *J. Climate,* **18,** 1253–1274.

LaRow, T. E., Y.-K. Lim, D. W. Shin, E. P. Chassignet, and S. Cocke, 2008: Atlantic basin seasonal hurricane simulations. *J. Climate,* **21,** 3191–3206.

Lavender, S. L., and K. J. E. Walsh, 2011: Dynamically downscaled simulations of Australian region tropical cyclones in current and future climates. *Geophys. Res. Lett.,* **38,** L10705, doi:10.1029/2011GL047499.

Li, L., W. Li, and Y. Deng, 2013: Summer rainfall variability over the southeastern United States in the 21st century as assessed by the CMIP5 models. *J. Geophys. Res. Atmos.,* **118,** 340–354, doi:10.1002/jgrd.50136.

Li, W., L. Li, R. Fu, Y. Deng, and H. Wang, 2011: Changes in the North Atlantic subtropical high and its role in the intensity of summer rainfall variability in the southeastern United States. *J. Climate,* **24,** 1499–1506.

Manabe, S., J. L. Holloway, and H. M. Stone, 1970: Tropical circulation in a time-integration of a global model atmosphere. *J. Atmos. Sci.,* **27,** 580–613.

McBride, J. L., 1984: Comments on ''Simulation on hurricane-type vortices in a general circulation model.'' *Tellus,* **36A,** 92–93.

McTaggart-Cowan, R., L. F. Bosart, C. A. Davis, E. H. Atallah, J. R. Gyakum, and K. A. Emanuel, 2006: Analysis of Hurricane Catarina (2004). *Mon. Wea. Rev.,* **134,** 3029–3053.

Meehl, G., C. Covey, T. Delworth, M. Latif, B. McAvaney, J. Mitchell, R. Stouffer, and K. Taylor, 2007: The WCRP CMIP3 multimodel dataset: A new era in climate change research. *Bull. Amer. Meteor. Soc.,* **88,** 1383–1394.

Menkes, C. E., M. Lengaigne, P. Marchesiello, N. C. Jourdain, E. M. Vincent, J. Lefèvre, F. Chauvin, and J.-F. Royer, 2012: Comparison of tropical cyclogenesis indices on seasonal to interannual timescales. *Climate Dyn.,* **38,** 301–321.

Mizuta, R., and Coauthors, 2012: Climate simulations using the improved MRI-AGCM with 20-km grid. *J. Meteor. Soc. Japan,* **90A,** 233–258.

Murakami, H., and M. Sugi, 2010: Effect of model resolution on tropical cyclone climate projections. *SOLA,* **6,** 73–76, doi:10.2151/sola.2010-019.

——, and B. Wang, 2010: Future change of North Atlantic tropical cyclone tracks: Projection by a 20-km-mesh global atmospheric model. *J. Climate,* **23,** 2699–2721.

——, R. Mizuta, and E. Shindo, 2012a: Future changes in tropical cyclone activity project by multi-physics and multi-SST ensemble experiments using 60-km-mesh MRI-AGCM. *Climate Dyn.,* **39,** 2569–2584.

——, and Coauthors, 2012b: Future changes in tropical cyclone activity projected by the new high-resolution MRI-AGCM. *J. Climate,* **25,** 3237–3260.

Neumann, C. J., B. R. Jarvinen, C. J. McAdie, and G. R. Hammer, 1999: Tropical cyclones of the North Atlantic Ocean, 1871-1998. National Climatic Data Center and Tropical Prediction Center/National Hurricane Center Rep., 206 pp.

Nolan, D. S., E. D. Rappin, and K. A. Emanuel, 2007: Tropical cyclogenesis sensitivity to environmental parameters in radiative-convective equilibrium. *Quart. J. Roy. Meteor. Soc.,* **133,** 2085–2107.

Oouchi, K., J. Yoshimura, H. Yoshimura, R. Mizuta, S. Kusunoki, and A. Noda, 2006: Tropical cyclone climatology in a global-warming climate as simulated in a 20-km-mesh global atmospheric model: Frequency and wind intensity analysis. *J. Meteor. Soc. Japan,* **84,** 259–276.

Pezza, A. B., and I. Simmonds, 2005: The first South Atlantic hurricane: Unprecedented blocking, low shear and climate change. *Geophys. Res. Lett.,* **32,** L15712, doi:10.1029/2005GL023390.

Ramsay, H. A., S. J. Camargo, and D. Kim, 2012: Cluster analysis of tropical cyclone tracks in the Southern Hemisphere. *Climate Dyn.,* **39,** 897–917.

Reed, K. A., and C. Jablonowski, 2011a: Impact of physical parametrization on idealized tropical cyclones in the Community Atmosphere Model. *Geophys. Res. Lett.,* **38,** L04805, doi:10.1029/2010GL046297.

——, and ——, 2011b: Assessing the uncertainty of tropical cyclone simulations in NCAR's Community Atmosphere Model. *J. Adv. Model. Earth Syst.,* **3,** M08002, doi:10.1029/2011MS000076.

——, and ——, 2012: Idealized tropical cyclone simulations of intermediate complexity: A test case for AGCMs. *J. Adv. Model Earth Syst.,* **4,** M04001, doi:10.1029/2011MS000099.

Rotstayn, L. D., S. J. Jeffrey, M. A. Collier, S. M. Dravitzki, A. C. Hirst, J. I. Syktus, and K. K. Wong, 2012: Aerosol- and greenhouse gas-induced changes in summer rainfall and circulation in the Australasian region: A study using single-forcing climate simulations. *Atmos. Chem. Phys.,* **12,** 6377–6404.

Sheffield, J., and Coauthors, 2013: North American climate in the CMIP5 experiments. Part II: Evaluation of historical simulations of intraseasonal to decadal variability. *J. Climate,* in press.

Smith, D., R. Eade, N. J. Dunstone, D. Fereday, J. M. Murphy, H. Pohlmann, and A. A. Scaife, 2010: Skilful multi-year predictions of Atlantic hurricane frequency. *Nat. Geosci.,* **3,** 846–849.

Smith, T. M., R. W. Reynolds, T. C. Peterson, and J. Lawrimore, 2008: Improvements to NOAA's historical merged land–ocean surface temperature analysis (1880–2006). *J. Climate,* **21,** 2283–2296.

Sobel, A. H., and S. J. Camargo, 2011: Projected future changes in tropical summer climate. *J. Climate,* **24,** 473–487.

Strachan, J., P. L. Vidale, K. Hodges, M. Roberts, and M.-E. Demory, 2013: Investigating global tropical cyclone activity with a hierarchy of AGCMs: The role of model resolution. *J. Climate,* **26,** 133–152.

Sugi, M., H. Murakami, and J. Yoshimura, 2009: A reduction in global tropical cyclone frequency due to global warming. *SOLA,* **5,** 164–167.

——, ——, and ——, 2012: On the mechanism of tropical cyclone frequency changes due to global warming. *J. Meteor. Soc. Japan,* **90A,** 397–408.

Taylor, K. E., R. J. Stouffer, and G. A. Meehl, 2012: An overview of CMIP5 and the experiment design. *Bull. Amer. Meteor. Soc.,* **93,** 485–498.

Tippett, M. K., S. J. Camargo, and A. H. Sobel, 2011: A Poisson regression index for tropical cyclone genesis and the role of large-scale vorticity in genesis. *J. Climate,* **24,** 2335–2357.

Vecchi, G. A., and B. J. Soden, 2007a: Increased tropical Atlantic wind shear in model projections of global warming. *Geophys. Res. Lett.,* **34,** L08702, doi:10.1029/2006GL028905.

——, and ——, 2007b: Effect of remote sea surface temperature change on tropical cyclone potential intensity. *Nature,* **450,** 1066–1070.

——, and ——, 2007c: Global warming and the weakening of the tropical circulation. *J. Climate,* **20,** 4316–4340.

——, ——, A. T. Wittenberg, I. M. Held, A. Leetmaa, and M. J. Harrison, 2006: Weakening of tropical Pacific atmospheric circulation due to anthropogenic forcing. *Nature,* **441,** 73–76.

——, and Coauthors, 2013: Multiyear predictions of North Atlantic hurricane frequency: Promise and limitations. *J. Climate,* **26,** 5337–5357.

Villarini, G., and G. A. Vecchi, 2012: Twenty-first-century projections of North Atlantic tropical storms from CMIP5 models. *Nat. Climate Change,* **2,** 604–607.

——, and ——, 2013: Projected increases in North Atlantic tropical cyclone intensity from CMIP5 models. *J. Climate,* **26,** 3231–3240.

——, ——, T. R. Knutson, M. Zhao, and J. A. Smith, 2011: North Atlantic tropical storms frequency response to anthropogenic forcing projections and sources of uncertainty. *J. Climate,* **24,** 3224–3238.

Vitart, F., 2009: Impact of the Madden Julian oscillation on tropical storms and risk of landfall in the ECMWF forecast system. *Geophys. Res. Lett.,* **36,** L15802, doi:10.1029/2009GL039089.

——, and T. N. Stockdale, 2001: Seasonal forecasting of tropical storms using coupled GCM integrations. *Mon. Wea. Rev.,* **129,** 2521–2537.

——, J. L. Anderson, and W. F. Stern, 1997: Simulation of interannual variability of tropical storm frequency in an ensemble of GCM integrations. *J. Climate,* **10,** 745–760.

——, ——, J. Sirutis, and R. E. Tuleya, 2001: Sensitivity of tropical storms simulated by a general circulation model to changes in cumulus parametrization. *Quart. J. Roy. Meteor. Soc.,* **127,** 25–51.

——, A. Leroy, and M. C. Wheeler, 2010: A comparison of dynamical and statistical predictions of weekly tropical cyclone activity in the Southern Hemisphere. *Mon. Wea. Rev.,* **138,** 3671–3682.

Voldoire, A., and Coauthors, 2013: The CNRM-CM5.1 global climate model: Description and basic evaluation. *Climate Dyn.,* **40,** 2091–2121, doi:10.1007/s00382-011-1259-y.

Volodin, E. M., N. A. Dianskii, and A. V. Gusev, 2010: Simulating present-day climate with INMCM4.0 coupled model of the atmospheric and oceanic general circulations. *Izv. Atmos. Oceanic Phys.,* **46,** 414–431.

Walsh, K. J. E., M. Fiorino, C. W. Landsea, and K. L. McInnes, 2007: Objectively determined resolution-dependent threshold criteria for the detection of tropical cyclones in climate model and reanalyses. *J. Climate,* **20,** 2307–2314.

——, S. Lavender, H. Murakami, E. Scoccimarro, L.-P. Caron, and M. Ghantous, 2010: The tropical cyclone climate model intercomparison. *Hurricanes and Climate Change,* Vol. 2, J. B. Elsner et al., Eds., Springer, 1–24.

——, ——, E. Scoccimarro, and H. Murakami, 2013: Resolution dependence of tropical cyclone formation in CMIP3 and finer resolution models. *Climate Dyn.,* **40,** 585–599.

Wang, H., J.-K. Schemm, A. Kumar, W. Wang, L. Long, M. Chelliah, G. D. Bell, and P. Peng, 2009: A statistical forecast model for Atlantic seasonal hurricane activity based on the NCEP dynamical seasonal forecast. *J. Climate,* **22,** 4481–4500.

Watanabe, M., and Coauthors, 2010: Improved climate simulation by MIROC5: Mean states, variability, and climate sensitivity. *J. Climate,* **23,** 6312–6335.

——, and Coauthors, 2011: MIROC-ESM: Model description and basic results of CMIP5-20c3m experiments. *Geosci. Model Dev. Discuss.,* **4,** 1063–1128.

Wing, A. A., A. H. Sobel, and S. J. Camargo, 2007: The relationship between the potential and actual intensities of tropical cyclones on interannual time scales. *Geophys. Res. Lett.,* **34,** L08810, doi:10.1029/2006GL028581.

Yokoi, S., and Y. N. Takayabu, 2009: Multi-model projection of global warming impact on tropical cyclone genesis frequency over the western North Pacific. *J. Meteor. Soc. Japan,* **87,** 525–538.

——, ——, and J. C. L. Chan, 2009: Tropical cyclone genesis frequency over the western North Pacific. *J. Meteor. Soc. Japan,* **87,** 525–538.

Yukimoto, S., and Coauthors, 2012: A new global climate model of the Meteorological Research Institute: MRI-CGCM3—Model description and basic performance. *J. Meteor. Soc. Japan,* **90A,** 23–64, doi:10.2151/jmsj.2012-A02.

Zanchettin, D., A. Rubino, D. Matei, O. Bothe, and J. H. Jungclaus, 2012: Multidecadal-to-centennial SST variability in the MPI-ESM simulation ensemble for the last millennium. *Climate Dyn.,* **39,** 419–444.

Zhang, Z. S., and Coauthors, 2012: Pre-industrial and mid-Pliocene simulations with NorESM-L. *Geosci. Model Dev.,* **5,** 523–533, doi:10.5194/gmd-5-523-2012.

Zhao, M., and I. M. Held, 2010: An analysis of the effect of global warming on the intensity of Atlantic hurricanes using a GCM with statistical refinement. *J. Climate,* **23,** 6382–6393.

——, ——, S.-J. Lin, and G. A. Vecchi, 2009: Simulations of global hurricane climatology, interannual variability, and response to global warming using a 50-km resolution GCM. *J. Climate,* **22,** 6653–6678.

——, ——, and ——, 2012: Some counterintuitive dependencies of tropical cyclone frequency on parameters in a GCM. *J. Atmos. Sci.,* **69,** 2272–2283.